Model of electrically stimulated hernia mesh electrode for soft tissue healing

By

Morgan Riley
B.Sc., Walla Walla University, 2015

Submitted to the graduate degree program in Bioengineering and the Graduate Faculty of the University of Kansas in partial fulfillment of the requirements for the degree of Master of Science.

_____
Chairperson: Dr. Elizabeth Friis

_____
Dr. Jennifer Robinson

_____
Dr. Sara Wilson

Date Defended: June 6, 2022

The Thesis Committee for Morgan Riley certifies that this is the approved version of the following thesis

Model of electrically stimulated hernia mesh electrode for soft tissue healing

_____

Chairperson: Dr. Elizabeth Friis

Date Approved: June 13, 2022

Abstract

Hernia repair is a common surgery that repairs tissues that have torn due to strain, allowing the internal organs to protrude from the body cavity [1,2]. Hernioplasty, which is hernia repair surgery with incorporation of a mesh to prevent retearing by mechanically supporting the tissues, has various levels of success. Factors such as infection, comorbidities, and age all play a role in how quickly the body can recover. To allow the tissues to be strengthened more naturally, an incorporation of electrical stimulation of the tissues would encourage faster cellular proliferation and therefore wound healing for strengthening the soft tissues [3]. An alternating current (AC) that creates an electric field in the region surrounding a wound has shown in other studies to encourage cellular proliferation and faster healing [3-5]. Previous related research utilized piezoelectric materials to output small amounts of voltage by stimulating the piezoelectric material [6]. This output voltage has been shown to be achievable in soft tissues through transcutaneous medically safe 1MHz ultrasound waves stimulation of the piezoelectric material that mimic the effect of mechanical loading [7]. A literature review of stimulation of cells within soft tissue indicates that fibroblasts proliferate within a sinusoidal AC electric field range of 20-300 mV/mm [3-6].

In this study, the output created by ultrasound loaded piezoelectric device was incorporated into a computational COMSOL® model of a conductive hernia mesh. COMSOL®, a multiphysics finite element analysis software, was used to model the conductive electrode, determine voltage inputs and their resulting electric fields, and to test designs for creating a clinically relevant electric field stimulation within the proliferation range for fibroblasts. The model shows an electrically stimulated hernia mesh devised from the current methods of implanted polypropylene (PP) hernia mesh, by overlaying a thin gold surface onto the polymer

mesh, which is proposed to be connected to a small piezoelectric device. For maximized area of stimulation, one of the electrode connection points is insulated from the body environment to conduct the positive and negative electrode points to opposite sides of the wound, creating an electric field across the wound site. Electrode materials for the mesh conductance layer were tested within the model, which showed similar electric fields for each material. The small differences were shown to be based on the material properties, which allowed higher or lower conductance through the surrounding solution, phosphate buffered saline. Gold was chosen to be the conductive metal based on its moderate electric field and biocompatibility. A range of possible output voltages from the piezoelectric device were also modeled in a voltage sweep to show the maximum and minimum electric fields the tissues would experience within the previously set range. When several set points in the electric field were measured at a value of V_{in}=100 mV, the electric field average was 5.93 ± 1.24. The overall electric field showed maximum values at the anode and cathode, but there was also stimulation midway between the nodes that could supply moderate stimulation to cells wherever they may lie within the electric field. It was concluded from these computations that a voltage of 20mV – 250mV should allow for increased tissue healing through cellular proliferation when connected to gold coated polypropylene hernia mesh.

Acknowledgments:

Dr. Elizabeth Friis

I would like to thank my advisor Dr. Lisa Friis for not only her advice on engineering and research, but also life lessons. She has been so patient with me as I navigated research and graduate school and work and has given me a great example of what it means to be a professional engineer.

Dr. Jennifer Robinson

I would like to thank Dr. Jenny Robinson for her guidance and patience and contribution to this research project. Although our interactions were mostly related to other engineering activities, she was a wonderful role model and a supportive faculty.

Dr. Sara Wilson

I would like to thank Dr. Sara Wilson for her willingness to participate in my thesis defense and for giving me advice on product development. I was only able to take one class from her, but she was a wonderful professor and made the very class enjoyable. It was always a pleasure to talk to her whenever we crossed paths.

My Lab Mates at University of Kansas

- **Tori Drapal, Savannah Mosier, Jordan Gamble, Chris Tacca, & James Egan**

I would like to thank all my lab mates in Dr. Friis' lab. You all were wonderful to work with and I will miss our eclectic conversations and our intense lab cleaning parties. You guys are what made the lab atmosphere welcoming and enjoyable.

My Friends and Fellow Graduate Students

- **Lexi Simar, Kara Hageman, Alyssa Curry, Victoria Blackwood, Aya Cloyd, & Phil Elrod**

I would like to thank my friends for accepting my weird self. When the days were especially rough, you guys were the ones who made life keep going. We celebrated the accomplishments, we commiserated in our pains, and we will continue to conquer another day. You guys are the absolute best and I do not think I would have enjoyed school nearly as much without you all.

My Family

I would like to thank my family for every supportive phone call, every letter, and every prayer they made on my behalf. It was not easy being so far apart, but your love and support and encouragement helped at every step of the way.

My Husband, Michael Riley

I would like to thank my husband Michael Riley for being with me through this process. He encouraged me when I felt down and pushed me to new limits and accomplishments I may not have reached for on my own. His respect and love kept me going every day.

Table of Contents:

List of Figures:

List of Tables:

Chapter 1: Introduction

1.1 Background and Motivation

In the United States, over a million patients develop a hernia every year that require surgical repair [1,2]. Hernias can develop in many different locations that require special care and treatment, depending on the location [3]. One of the most common hernias is the ventral hernia, which is typically repaired by use of hernia mesh placed between the abdominis muscles and the transverse fascia, known as sublay method [3]. Over the years, the treatment methods for hernias have changed from simple sutures to supportive hernia mesh, to bioabsorbable mesh and other native tissue materials [3,4]. And even if the surgery went well, the common long-term issues could vary between occasional to chronic pain at the hernia site, severed nerves that result in loss of sensation, or complete retearing of the hernia [3]. Regardless of the type of hernia, 63% of hernias surgically repaired will experience a recurrence, which is a retearing of the already weakened site [5]. When a mesh is present to support the weakened region, however, recurrence is only seen in 32% or less [6,7]. Some patients who experience recurrence are individuals who already had comorbidities that put them more at risk, but anyone can get an infection from surgical implantation of a medical device that is not native to the body. Considering the number of individuals who require hernia repair are increasing with each year, finding a method of further reducing problems with mesh implantation would significantly impact patient recovery and further reduce recurrence rates.

As with most medical device implants, the main issues seen with hernia mesh repair are infection, inflammation, and effective healing. Tissues adhering to the mesh and chronic pain are also seen in certain mesh brands and designs [4]. An ideal implant would have no complications with tissue acceptance and a patient would have no long-term pain in the region or recurrence.

Hernia mesh has come a long way in its development for effective hernia treatment, but the number of recurrences could be decreased by utilizing newer methods and discoveries. Infection could be mitigated in part by faster wound healing. Inflammation is often a result of tissue rejection of the materials used. Hernia mesh's porosity also comes into play with inflammation if granulomas form in the tissue around the mesh [7-9]. All these issues may be not able to be addressed with one solution, but they should be addressed.

Years ago, a man named Theodor Billroth, a renowned Austrian surgeon and considered in many ways to be the father of abdominal surgery as we know it today, understood the need to continue pushing for better hernia treatments. In 1878 he stated, "If we could artificially produce tissues of the density and toughness of fascia and tendon, the secret of the radical cure of hernia would be discovered" [10]. It has been almost a hundred and fifty years since then, and science still has not achieved what Billroth proposed. Millions of people worldwide have undergone hernia repair surgery and the issues surrounding hernia repair should not be an acceptable outcome for a patient to live with for the rest of their lives. But until science has developed a method and surgical practice to mitigate the typical hernia complaints, Billroth's dream will not be realized.

1.2 Specific Aims

Despite there being several complications associated with hernia repair, not all of them can be mitigated by one solution. The goal of this research is to propose a model of hernia repair mesh that incorporates a metal conductive layer for soft tissue electrical stimulation through the incorporation of piezoelectric device. By adding an electrical current across the mesh, an electric field would be introduced to the region for cellular stimulation. The piezoelectric device would be stimulated by a therapeutic and medically safe ultrasound wave that creates the device voltage

output. A possible range of voltage output amplitudes will also be determined to promote safe and positive cellular stimulation. The design of the electrode is important because it controls the conduction direction of flow and where the piezoelectric device would connect to in order to achieve the desired electric field. By using COMSOL®, a metaphysics finite element analysis software, a comparison of several conductive materials will be done to find the best material is chosen to create an electric field that evenly stimulates the cells in a future *in vitro* study. The different materials have different characteristics that include conductance and relative permittivity, which directly impact how an electric field forms around the electrode. Phosphate buffered saline (PBS) will serve as the *in vitro* solution for the COMSOL® outer boundary conditions the electric field passes through.

Chapter 2: Background, Significance and Literature Review

2.1 Hernia Repair

2.1.1 History of Hernia Repair

The first record of hernia repair surgery dates to 1552 BC in ancient Egypt and mostly evolved from the need to treat battle wounds [11,12]. Hernias, as we know them, would have been an ailment the common person would have experienced outside of battle wounds as well. The word "hernia" has Latin origins and was meant to describe a "prolapse," which is when an organ or part of the body is displaced from where it should be located, often resulting in a protrusion (Figure 1) [3,13].

Figure 1. Diagram general abdominal hernia prolapse.

Many surgeons documented work in the 18th century that aimed towards a method of herniorrhaphy (repairing hernias by suture), but it was not until 1887 that the modern technique of herniorrhaphy was developed by a man named Edoardo Bassini [14]. Bassini realized that the methods at the time were not treating the main issue, which he saw to be the anatomy and physiology around the hernias and not the technique [15]. By reconstructing each hernia and the inguinal canal tissues based on their specific anatomy, Bassini was able to show the world that patients with hernias can make full recoveries [14,15]. The next major step for hernia repair came in the 20th century through Theodore Billroth, who introduced the idea of using other materials to support the tissues in a "tension free" repair [15]. Several materials were

experimented with, but it was not until 1958 that Francis Usher used polypropylene: the first polymer to successfully be used as hernia mesh [4].

2.1.2 Mesh Materials

The materials currently used in hernia repair are typically various polymers and their combinations. Nylon and some woven metals were also tried over the years with varying success. As Billroth had stated, a successful mesh material must match the "density and toughness of fascia and tendon" [10]. Newer methods of mesh testing have revealed that surface chemistry and pore size also play a large part in tissue acceptance [4,7]. Besides the permanent mesh materials, biodegradable polymers and biological scaffolds have also shown success in current hernia repair [4]. With so many materials to choose from, surgeons' preferences vary not only on their individual experiences, but also on the needs of the patient [16]. And even though surgeons can pick the best option for their patient, recurrence is still frequently seen.

2.1.3 Surgical Techniques

Hernia repair surgical methods have changed drastically over the years, but the main goal has not. The goal is to repair the patient's body cavity wall so that the tissues go back to their normal state, both anatomically and physiologically, and with the expectation that the hernia should not retear [12].

As mentioned previously, herniorrhaphy is the classic method of repairing hernias by suture alone. Hernioplasty is the modern version of hernia repair that utilizes mesh in surgery to support the tissues [3]. As technology became more advanced in the 20th century, laparoscopic surgery came into the picture [15,17]. Laparoscopic surgery utilizes small entry ports to access the wound while viewing the procedure through a small camera inserted into the working site. For safe and effective surgery and results, this requires the surgeon to not only have high

technical skills to control the devices, but also requires they are very familiar with the anatomical layers around the hernia [17]. Both open surgery hernioplasty and laparoscopic surgery utilize hernia mesh, and there are different ways in which these can be performed. The variations are based on which tissue layers, or plane, the mesh is placed between, and there are several layers to the abdominal wall (skin, fat, external oblique muscle, internal oblique muscle, transversus abdominus muscle, transverse fascia, extraperitoneal fascia, and peritoneum) for surgeons to work between [3]. A mesh placed between the fat layer and the muscles is called onlay/overlay method, mesh placed between the sides of the hernia defect is called inlay method, mesh placed between the abdominis muscles and the transverse fascia is called sublay method, and mesh placed between the fascia and peritoneum is called underlay method (Figure 2)[18]. Each method has its merits and faults, but sublay and underlay method are more commonly used [16]. Besides the choices in surgical method, there is also the choice in fixation device (sutures, tack, glue, suture-less) that each impact the tissues and the outcome of the hernia repair [3].

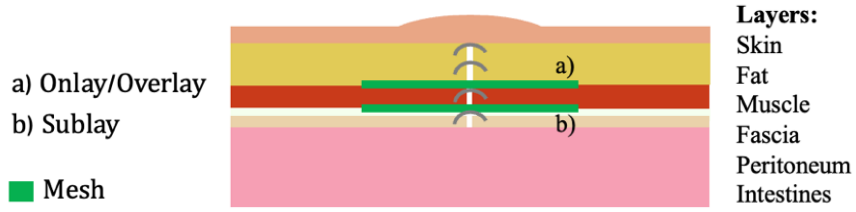

Figure 2. Simplified hernioplasty mesh placement diagram

There is no doubt that hernia repair is on the road to fewer recurrences and overall success. One surgeon, however, noted in the late 1990's that with all of the methods and options and successes and discrepancies between surgeons' personal experiences being recorded, the reviews at the time showed the overall recurrences was high, regardless of method or material used [19]. Today hernias, as simple and as common as they may be, still create lifelong issues for the average person.

2.1.4 Mesh Complications

The complications associated with hernia repair surgery fall in line with many of the typical issues expected in an invasive surgery. There are others, however, that are specific to the hernia region. Risk of infection or tissue inflammation, for example, are common to all surgeries and may require the implanted mesh to be removed before the surgery can be reattempted. In many hernioplasty cases, tissue inflammation is caused by the tissues trying to integrate and heal across the mesh, but due to the small pore size, granulomas form around the mesh. These granulomas are associated with foreign body response inflammation and are due to the tissues not being able to integrate with the mesh [7]. Another issue specific to hernia repair is when the mesh mechanical properties do not match the tissues it is trying to support [20,21]. A review by Sanbhal et al. (2017) found that light weight and heavy weight meshes had elasticities of 30% and 15% respectively at a force of 16 N/cm, while tissues can experience a maximum 38% elasticity at 26 N/cm of force [9]. The range of 15-30% elasticity in mesh was noted to produce favorable results in hernia repair [9]. In the extremes where the mesh materials are too elastic compared to the tissues, the muscle fibers and collagen at the site could overstretch and cause a recurrence. If the mesh is too rigid, the sutured anchor points pull on the tissues and can cause a recurrence [7-9,18].

Another complication associated with most medical implants, as well as hernia mesh, is tissue adhesion due to the surface biochemistry of the implant material. The characteristic of being hydrophobic is desirable in many hernia meshes due to the limitation of functional groups and low surface energy that reduces the ability of tissues to adhere to the mesh [9,22-25]. Arnaud et al. (2003) notes that if the tissues adhere to the mesh, the proximity of the mesh to the intestines often results in the adhering tissue being the intestines, which may result in major

complications such as bowel obstruction [26]. Additionally, if the tissues are agitated to the point that scar tissue is incited to form, oxidants are released by the tissues which can degrade polymer mesh over time due to oxidization and fouling [5]. This mesh degradation continues the adverse tissue response, resulting in chronic pain, scar tissue, and embrittlement or shrinking of the mesh and eventual hernia recurrence [5].

Despite the simplicity of hernias in comparison to other surgeries, the biochemistry of the implanted materials is important for short- and long-term patient quality of life and ensuring minimal complications. Given all the different complications a hernia repair patient may experience, hernioplasty could benefit from a method that not only strengthens the tissues but also decreases healing time. This result could be achieved through cellular proliferation in the hernia region from an external stimulation.

2.2 Electrical Stimulation

2.2.1 Cellular Proliferation

Within all parts of the body, there is an endogenous electric field (EF). This electric field is created within the tissues by cellular membrane electron potential differences, which function most notably in cellular communications and nerve impulses [27]. The endogenous EF plays a critical part in wound healing and healthy organism growth, and it ranges from a few mV/mm to hundreds of mV/mm, depending on the tissue and need [27,28]. Skin wounds, for an example of soft tissue, show an endogenous EF of 100-200 mV/mm [27]. Research by Kotnik and Miklavčič (2006) found that, if an external EF is added to cells *in vitro*, electroporation of the cellular membrane was induced [29]. Electroporation opens the normally closed cell membranes. This method of electrical stimulation Chen et al. (2019) notes can promote cellular communication, proliferation, and differentiation [30]. Despite the promoted proliferation and differentiation, it is

important that the EF strength and duration be within the limits of the specific cells receiving the stimulation to ensure tissues are not killed.

Before adding an electrical stimulation to hernia repair, tissue type and expected cells in the area need to be identified. For a soft tissue healing application, such as hernia repair, there are several types of tissues present (i.e. skin, muscle, fascia, peritoneum). One thing all these tissues require to heal is an extra cellular matrix (ECM) across the wounded region, which is the main function of fibroblasts [31,32]. Injured dermis naturally incites fibroblasts to quickly proliferate and fill the wound site with new ECM, which allows the other cells to then integrate and heal the region [33,34]. Injured muscle also utilizes fibroblasts, but through their differentiation. Buckley (2021) found that new muscle cells formed after an injury differentiated directly from fibroblasts [35]. Mendias (2017) also states that fibroblasts play an important role in muscle healing, but by guiding satellite cells (resident skeletal muscle stem cells) to severe muscle wounds [36,37]. Because fibroblasts are a cell line that factors into many areas of wound healing, targeting them as the distinct cell/tissue type for proliferation should aid in hernia recovery and possibly tissue strengthening.

2.2.2 Electric Field Stimulation

Since electrical stimulation can, at some point, do more harm than good, it is important to note the type and range of current a hernia mesh electrode would require to be effective. The goal is to amplify the cellular proliferation around the hernia wound, which should strengthen the tissues and reduce recurrence, decreasing healing time and chance of infection post-surgery. Current comes in two forms: direct current (DC) and alternating current (AC). Both currents are used in cellular stimulation, but they affect the target cells differently depending on cell type and electric field intensity. Thrivikraman et al. (2018) found that a DC electric field of 1400 mV/mm

caused mouse fibroblasts to migrate towards the cathode, but a DC electric field <30 mV/mm was noted to induce cell migration in pluripotent stem cells [27]. Thrivikraman et al. (2018) further noted that for wound healing, only low AC frequency electric fields should be used [27]. Since induced pluripotent stem cells (iPSC) can be derived from fibroblasts, it is worth noting that Chen et al. (2019) found AC frequency of 1Hz and an electric field between 65-200 mV/mm promoted cellular proliferation in iPSC [34,41]. Bhang et al. (2016) states the AC voltage range they found for wound healing was 150-1200 mV, and furthermore, they found in their *in vitro* study that an AC frequency of 0.5 Hz and a wave amplitude of 900 mV increased fibroblast proliferation and differentiation to myofibroblasts for dermal wound healing [38]. Their later *in vivo* study utilized a piezoelectric wrap that output a movement dependent frequency of 320-900 mV wave amplitude, which also showed increased wound healing [38]. Another study by Rouabia et al. (2013) noted that fibroblasts showed greater numbers and faster wound integration when exposed to an AC EF frequency of 50-60 Hz than fibroblasts that did not have any stimulation [39]. Based on this knowledge, it is reasonable to expect similar results if an EF was incorporated into a hernia mesh wound.

Without electrical stimulation, a wound directs cells towards itself through the endogenous EF [39-41]. An addition of an external electrical stimulation could then increase this effect. Despite the differences in AC and DC's range for proliferation in the various studies noted, the research shows that electrical stimulation of tissues aids in wound healing through different cells and pathways [27,39,42,43]. Because DC has a distinct polarity, DC can pull cells toward the anode or cathode across a wound. AC, on the other hand, uses an alternating polarity that encourages proliferation without forcefully moving the cells from their original location [27,39,42,43]. For the purposes of this study and with proliferation and strengthening of the soft

tissues being the goal, AC will be used, and a target electric field range of 20-300 mV/mm will be considered the proliferation range for soft tissue healing through the promotion of fibroblasts.

2.2.2.1 Electric Field Effects on Fibroblasts

Although research has shown that fibroblasts can be stimulated for proliferation through an EF, it is also worth noting that other amplified aspects of fibroblasts have also been seen that are beneficial to wound healing. A study by Rouabhia et al. (2013) studied the effect of electrical stimulation of fibroblasts for the specific goal of determining how their stimulation effects wound healing [39]. Not only did the fibroblasts migrate to fill the wound more quickly, but they also overall decreased the healing time of the wounds [39]. As to the reason of how they decreased healing time, this was partly due to the amplification of secreted FGF-1 and FGF-2 (fibroblast growth factor) and the contraction of collagen around the wound [39,41]. FGF's trigger fibroblast growth and migration to aid in wound healing. FGF secretion was hypothesized in this Rouabhia et al. (2013) study to be due to how the EF effects the cell's internal functions, through stimulation of gap-junctions for communication and increasing the cyclic AMP pathway [39]. FGFs also trigger fibroblasts to differentiate into myofibroblasts, which contributes to the increased ECM production and matrix contraction [39, 40]. As the matrix around the wound contracts, the wound size is reduced, aiding in tissue repair [39,40]. To summarize, the electrical stimulation of fibroblasts directly encourages cellular proliferation, but in addition, the fibroblasts in the region are triggered to aid in the wound healing through FGF-1,2 and their differentiation into myofibroblasts for reducing the wound size and producing ECM for cells to reintegrate into the wound area.

For the purposes of this study, the further reduction of recurrence is the goal. Most hernia wounds repaired by hernioplasty fully recover after three months but only regain up to 80% of

their original tensile strength [41]. Without a 100% restoration, recurrence is possible. Fibroblasts produce the materials that make up the ECM that contribute to this tissue strength. Kendall and Feghali-Bostwick (2014) notes that collagen type 1 is one fiber in the ECM that gives tensile strength, while elastin's crosslinked network allows the tissues to retain their elastic capabilities [40]. So, while studies on electrical stimulation of fibroblasts have not yet shown to what degree the specific proteins in the ECM are made when fibroblasts are stimulated, it can at least be seen that the fibroblasts proliferation and general ECM creation could be a factor for increasing the strength in the tissue region around the hernia site.

2.2.3 Circuit Current Density

Since a voltage and current will be required to create an electric field, previous work on this research topic for hernia repair should be taken into consideration. Norman (2021) looked at current density and its impact on generating a voltage across the mesh electrode and utilized a target current density of at least 85 nA/cm^2 to provide enhanced healing from an electrode with a surface area of 39.87 cm^2 [44]. They determined their theoretical current density based on measured resistance and voltage [44]. While this current density output would create a voltage and an EF, the current density will not be directly taken into consideration in this study. It should be noted that as the electrode surface area, resistance, and distance between anode and cathode points decreases, current density will increase, and vice versus if the surface area increased. This is because the current across the mesh electrode surface area determines the current density output. Direct cellular/tissue contact with the electrode and the effects on proliferation will also not be considered for this study.

2.3 Piezoelectricity

2.3.1 Piezoelectric Materials

To create the current and voltage for the cellular stimulation, an electric source is required. Piezoelectric materials are unique in that when placed under mechanical loading (compression/tension), they output an electric current. Piezoelectric materials were first discovered in the 19th century as naturally occurring crystals [45]. The current and resulting voltage they produce is due to the crystalline structure that would have been created by electric charges aligning the molecules into dipole moments before solidification. If the piezoelectric materials are compressed in line with the molecular alignment, the material sends out the electric current. There are many different piezoelectric materials today since they can now be artificially created by forcefully polarizing crystals during formation [45]. The specific material considered for this study is lead zirconate titanate (PZT), utilizing previous research voltage outputs by Norman (2021) as a baseline for a possible range of cellular stimulation [44].

2.3.2 Piezoelectric Power Generation

Since piezoelectric materials can output a current by harnessing their inner dipoles as they are stretched or compressed, the materials are perfect candidates for use in medical devices where movement is prevalent and healing via electric field is needed. Research studies have already shown in several applications how this is achievable [38,46,47]. One of the interesting characteristics of piezoelectrics and their application in medical devices is that they do not require a battery. Other devices require regular invasive surgery to change batteries, which can be large and undesirable for *in vivo* use. A small piece of piezoelectric material could be harnessed instead.

2.4 Ultrasound Stimulation

2.4.1 Ultrasound Parameters

Mechanical loading is not the only method of stimulating an output from piezoelectric materials. Ultrasound waves, which are high frequency sound waves, also elicit the same current and voltage from the piezoelectric materials. This is particularly of use when piezoelectric materials are placed in the body where movement and mechanical forces are not interacting strongly with the material, such as in soft abdominal tissues. It is important to note that the higher the frequency of the ultrasound wave hitting the piezoelectric material, the faster the oscillating output from the piezoelectric material will be [44]. Therapeutic ultrasound operates at a frequency of 0.7-3 MHz, which is safe and commonly used, whereas imaging and diagnostic ultrasound frequencies are typically higher and range from 1-20 MHz [48]. The higher frequencies for imaging are also safe, but usually used for shorter periods of time. When it comes to the frequency used for internal device stimulation for an expected current output, 1 MHz should provide ample current for use in cellular stimulation [44].

2.5 References

1. CDRH: Center for Devices and Radiological Health, Hernia surgical mesh implants, U.S. Food and Drug Administration. (n.d.). https://www.fda.gov/medical-devices/implants-and-prosthetics/hernia- surgical-mesh-implants (accessed October 13, 2021).

2. Kulacoglu, H. (2015). Current options in umbilical hernia repair in adult patients. *Turkish Journal of Surgery*. https://doi.org/10.5152/ucd.2015.2955

3. Hori, T., & Yasukawa, D. (2021). Fascinating history of groin hernias: Comprehensive recognition of anatomy, classic considerations for Herniorrhaphy, and current controversies in Hernioplasty. *World Journal of Methodology*, *11*(4), 160–186. https://doi.org/10.5662/wjm.v11.i4.160

4. Baylón, K., Rodríguez-Camarillo, P., Elías-Zúñiga, A., Díaz-Elizondo, J., Gilkerson, R., & Lozano, K. (2017). Past, present and future of surgical meshes: A Review. *Membranes*, *7*(3), 47. https://doi.org/10.3390/membranes7030047

5. Costello, C. R., Bachman, S. L., Ramshaw, B. J., & Grant, S. A. (2007). Materials characterization of explanted polypropylene hernia meshes. *Journal of Biomedical Materials Research Part B: Applied Biomaterials*, *83B*(1), 44–49. https://doi.org/10.1002/jbm.b.30764

6. Burger, J. W. A., Luijendijk, R. W., Hop, W. C. J., Halm, J. A., Verdaasdonk, E. G. G., & Jeekel, J. (2004). Long-term follow-up of a randomized controlled trial of suture versus mesh repair of incisional hernia. *Annals of Surgery*, *240*(4), 578–585. https://doi.org/10.1097/01.sla.0000141193.08524.e7

7. Wang See, C., Kim, T., & Zhu, D. (2020). Hernia mesh and hernia repair: A Review. *Engineered Regeneration*, *1*, 19–33. https://doi.org/10.1016/j.engreg.2020.05.002

8. Heymann, F., von Trotha, K.-T., Preisinger, C., Lynen-Jansen, P., Roeth, A. A., Geiger, M., Geisler, L. J., Frank, A. K., Conze, J., Luedde, T., Trautwein, C., Binnebösel, M., Neumann, U. P., & Tacke, F. (2019). Polypropylene mesh implantation for hernia repair causes myeloid cell–driven persistent inflammation. *JCI Insight*, *4*(2). https://doi.org/10.1172/jci.insight.123862

9. Sanbhal, N., Miao, L., Xu, R., Khatri, A., & Wang, L. (2017). Physical structure and mechanical properties of knitted hernia mesh materials: A Review. *Journal of Industrial Textiles*, *48*(1), 333–360. https://doi.org/10.1177/1528083717690613

10. Bredikhin, M., Gil, D., Rex, J., Cobb, W., Reukov, V., & Vertegel, A. (2020). Anti-inflammatory coating of hernia repair meshes: A 5-rabbit study. *Hernia*, *24*(6), 1191–1199. https://doi.org/10.1007/s10029-020-02122-9

11. Dobanovacki, D., Milovanovic, L., Slavkovic, A., Tatic, M., Miskovic, S., Skoric-Jokic, S., & Pecanac, M. (2012). Surgery before common era (B.C.E.). *Archive of Oncology*, *20*(1-2), 28–35. https://doi.org/10.2298/aoo1202028d

12: *History of hernia: Premier health*. History of Hernia | Premier Health. (n.d.). Retrieved March 10, 2022, from http://www.premierhealth.com/gem-city-surgeons/services/history-of-hernia

13. Merriam-Webster. (n.d.). *Prolapse definition & meaning*. Merriam-Webster. Retrieved March 10, 2022, from http://www.merriam-webster.com/dictionary/prolapse

14. Thomas, A. D., & Rogers, A. (2004). Edoardo Bassini and the wound that inspires. *World Journal of Surgery*, *28*(10), 1060–1062. https://doi.org/10.1007/s00268-004-7466-5

15. Komorowski, A. L. (2014, June 4). *Chapter: History of the inguinal hernia repair*. IntechOpen. Retrieved May 10, 2022, from https://www.intechopen.com/chapters/46621

16. Berbel, G. (2021). *Hernia - 101*. *Hernia Repair Research Project*. Lawrence; University of Kansas.

17. Yasukawa, D., Aisu, Y., & Hori, T. (2020). Crucial anatomy and technical cues for laparoscopic transabdominal preperitoneal repair: Advanced manipulation for groin hernias in adults. *World Journal of Gastrointestinal Surgery*, *12*(7), 307–325. https://doi.org/10.4240/wjgs.v12.i7.307

18. Parker, S. G., Wood, C. P., Sanders, D. L., & Windsor, A. C. (2017). Nomenclature in abdominal wall hernias: Is it time for consensus? *World Journal of Surgery*, *41*(10), 2488–2491. https://doi.org/10.1007/s00268-017-4037-0

19. Brandon, W. J. (1946). Inguinal hernia the unpredictable result. *British Journal of Surgery*, *34*(133), 13–18. https://doi.org/10.1002/bjs.18003413303

20. Anurov, M. V., Titkova, S. M., & Oettinger, A. P. (2011). Biomechanical compatibility of surgical mesh and fascia being reinforced: Dependence of experimental hernia defect repair results on anisotropic surgical mesh positioning. *Hernia*, *16*(2), 199–210. https://doi.org/10.1007/s10029-011-0877-y

21. Grasa, J., Sierra, M., Lauzeral, N., Muñoz, M. J., Miana-Mena, F. J., & Calvo, B. (2016). Active behavior of abdominal wall muscles: Experimental results and numerical model formulation. *Journal of the Mechanical Behavior of Biomedical Materials*, *61*, 444–454. https://doi.org/10.1016/j.jmbbm.2016.04.013

22. Lu, X., Khanna, A., Luzinov, I., Nagatomi, J., & Harman, M. (2018). Surface modification of polypropylene surgical meshes for improving adhesion with Poloxamine Hydrogel adhesive. *Journal of Biomedical Materials Research Part B: Applied Biomaterials*, *107*(4), 1047–1055. https://doi.org/10.1002/jbm.b.34197

23. Engelsman, A. F., van Dam, G. M., van der Mei, H. C., Busscher, H. J., & Ploeg, R. J. (2010). In vivo evaluation of bacterial infection involving morphologically different surgical meshes. *Annals of Surgery*, *251*(1), 133–137. https://doi.org/10.1097/sla.0b013e3181b61d9a

24. Shokrollahi, M., Bahrami, S. H., Nazarpak, M. H., & Solouk, A. (2020). Biomimetic double-sided polypropylene mesh modified by DOPA and ofloxacin loaded carboxyethyl chitosan/polyvinyl alcohol-polycaprolactone nanofibers for potential hernia repair applications. *International Journal of Biological Macromolecules*, *165*, 902–917. https://doi.org/10.1016/j.ijbiomac.2020.09.229

25. Auriemma, F., Ruiz de Ballesteros, O., De Rosa, C., & Invigorito, C. (2011). Tailoring the mechanical properties of isotactic polypropylene by blending samples with different stereoregularity. *Macromolecules*, *44*(15), 6026–6038. https://doi.org/10.1021/ma201420f

26. Arnaud, J. P., Hennekinne-Mucci, S., Pessaux, P., Tuech, J. J., & Aube, C. (2003). Ultrasound detection of visceral adhesion after intraperitoneal ventral hernia treatment: A comparative study of protected versus unprotected meshes. *Hernia*, *7*(2), 85–88. https://doi.org/10.1007/s10029-003-0116-2

27. Thrivikraman, G., Boda, S. K., & Basu, B. (2018). Unraveling the mechanistic effects of electric field stimulation towards directing stem cell fate and function: A tissue engineering perspective. *Biomaterials*, *150*, 60–86. https://doi.org/10.1016/j.biomaterials.2017.10.003

28. Levin, M. (2014). Molecular bioelectricity: How endogenous voltage potentials control cell behavior and instruct pattern regulation in vivo. *Molecular Biology of the Cell*, *25*(24), 3835–3850. https://doi.org/10.1091/mbc.e13-12-0708

29. Kotnik, T., & Miklavčič, D. (2006). Theoretical evaluation of voltage inducement on internal membranes of biological cells exposed to electric fields. *Biophysical Journal*, *90*(2), 480–491. https://doi.org/10.1529/biophysj.105.070771

30. Chen, C., Bai, X., Ding, Y., & Lee, I.-S. (2019). Electrical stimulation as a novel tool for regulating cell behavior in tissue engineering. *Biomaterials Research*, *23*(1). https://doi.org/10.1186/s40824-019-0176-8

31. Schäfer, M., & Werner, S. (2007). Transcriptional control of wound repair. *Annual Review of Cell and Developmental Biology*, *23*(1), 69–92. https://doi.org/10.1146/annurev.cellbio.23.090506.123609

32. Chang, Y., Li, H., & Guo, Z. (2014). Mesenchymal stem cell-like properties in fibroblasts. *Cellular Physiology and Biochemistry*, *34*(3), 703–714. https://doi.org/10.1159/000363035

33. Fronza, M., Heinzmann, B., Hamburger, M., Laufer, S., & Merfort, I. (2009). Determination of the wound healing effect of calendula extracts using the scratch assay with 3T3 fibroblasts. *Journal of Ethnopharmacology*, *126*(3), 463–467. https://doi.org/10.1016/j.jep.2009.09.014

34. *Fibroblast*. Fibroblast | Cell Applications. (n.d.). Retrieved May 25, 2022, from https://www.cellapplications.com/fibroblast

35. Buckley, C. D. (2021). Fibroblast cells reveal their ancestry. *Nature*, *593*(7860), 511–512. https://doi.org/10.1038/d41586-021-01204-7

36. Mendias, C. L. (2017). Fibroblasts take the centre stage in human skeletal muscle regeneration. *The Journal of Physiology*, *595*(15), 5005–5005. https://doi.org/10.1113/jp274403

37. Laumonier, T., & Menetrey, J. (2016). Muscle injuries and strategies for improving their repair. *Journal of Experimental Orthopaedics*, *3*(1). https://doi.org/10.1186/s40634-016-0051-7

38. Bhang, S. H., Jang, W. S., Han, J., Yoon, J.-K., La, W.-G., Lee, E., Kim, Y. S., Shin, J.-Y., Lee, T.-J., Baik, H. K., & Kim, B.-S. (2016). Zinc oxide nanorod-based piezoelectric dermal patch for wound healing. *Advanced Functional Materials*, *27*(1), 1603497. https://doi.org/10.1002/adfm.201603497

39. Rouabhia, M., Park, H., Meng, S., Derbali, H., & Zhang, Z. (2013). Electrical stimulation promotes wound healing by enhancing dermal fibroblast activity and promoting myofibroblast transdifferentiation. *PLoS ONE*, *8*(8). https://doi.org/10.1371/journal.pone.0071660

40. Kendall, R. T., & Feghali-Bostwick, C. A. (2014). Fibroblasts in fibrosis: Novel roles and mediators. *Frontiers in Pharmacology*, *5*. https://doi.org/10.3389/fphar.2014.00123

41. Sadava, E. E., Krpata, D. M., Gao, Y., Rosen, M. J., & Novitsky, Y. W. (2013). Wound healing process and mediators: Implications for modulations for hernia repair and mesh integration. *Journal of Biomedical Materials Research Part A*, *102*(1), 295–302. https://doi.org/10.1002/jbm.a.34676

42. Guo, A., Song, B., Reid, B., Gu, Y., Forrester, J. V., Jahoda, C. A. B., & Zhao, M. (2010). Effects of physiological electric fields on migration of human dermal fibroblasts. *Journal of Investigative Dermatology*, *130*(9), 2320–2327. https://doi.org/10.1038/jid.2010.96

43. Barki, K. G., Das, A., Dixith, S., Ghatak, P. D., Mathew-Steiner, S., Schwab, E., Khanna, S., Wozniak, D. J., Roy, S., & Sen, C. K. (2019). Electric field based dressing disrupts mixed-species bacterial biofilm infection and restores functional wound healing. *Annals of Surgery*, *269*(4), 756–766. https://doi.org/10.1097/sla.0000000000002504

44. Norman, A. (2021). *Determination of a Clinically Relevant Tissue Phantom for Transcutaneous Ultrasound Stimulation of Piezoelectric Discs for Current Density Applications* (thesis). University of Kansas, Lawrence.

45. APC International, L., *Piezoelectric Ceramics: Principles and Applications.* APC International., 2021.

46. Dagdeviren, C., Shi, Y., Joe, P., Ghaffari, R., Balooch, G., Usgaonkar, K., Gur, O., Tran, P. L., Crosby, J. R., Meyer, M., Su, Y., Chad Webb, R., Tedesco, A. S., Slepian, M. J., Huang, Y., & Rogers, J. A. (2015). Conformal piezoelectric systems for clinical and experimental characterization of soft tissue biomechanics. *Nature Materials*, *14*(7), 728–736. https://doi.org/10.1038/nmat4289

47. Long, Y., Wei, H., Li, J., Yao, G., Yu, B., Ni, D., Gibson, A. L. F., Lan, X., Jiang, Y., Cai, W., & Wang, X. (2018). Effective wound healing enabled by discrete alternative electric fields from wearable nanogenerators. *ACS Nano*, *12*(12), 12533–12540. https://doi.org/10.1021/acsnano.8b07038

48. Ahmadi, F., McLoughlin, I. V., Chauhan, S., & ter-Haar, G. (2012). Bio-effects and safety of low-intensity, low-frequency ultrasonic exposure. *Progress in Biophysics and Molecular Biology*, *108*(3), 119–138. https://doi.org/10.1016/j.pbiomolbio.2012.01.004

Chapter 3: Journal Article

This section contains a manuscript to be submitted for publication with the Journal of Medical Devices Tech Notes

Title:

Model of electrically stimulated hernia mesh and measurements of electric field for soft tissue healing using COMSOL Multiphysics®.

Authors:

Morgan Riley
Spine Biomechanics Laboratory,
Department of Bioengineering,
University of Kansas,
Lawrence, KS 66045
Email: morgan.riley@ku.edu

Dr. Elizabeth Friis
Professor,
Department of Mechanical Engineering,
University of Kansas,
Lawrence, KS 66045
Email: lfriis@ku.edu

3.1 Abstract

Hernia repair is a common surgery that repairs tissues that have torn due to strain, allowing the internal organs to protrude from the body cavity [1,2]. Hernioplasty, which is hernia repair surgery with incorporation of a mesh to prevent retearing by mechanically supporting the tissues, has various levels of success. Factors such as infection, comorbidities, and age all play a role in how quickly the body can recover. To allow the tissues to be strengthened more naturally, an incorporation of electrical stimulation of the tissues would encourage faster cellular proliferation and therefore wound healing for strengthening the soft tissues [3]. An alternating current (AC) that creates an electric field in the region surrounding a wound has shown in other studies to encourage cellular proliferation and faster healing [3-5]. Previous related research utilized piezoelectric materials to output small amounts of voltage by stimulating the piezoelectric material [6]. This output voltage has been shown to be achievable in soft tissues through transcutaneous medically safe 1MHz ultrasound waves stimulation of the piezoelectric material that mimic the effect of mechanical loading [7]. A literature review of stimulation of cells within soft tissue indicates that fibroblasts proliferate within a sinusoidal AC electric field range of 20-300 mV/mm [3-6].

In this study, the output created by ultrasound loaded piezoelectric device was incorporated into a computational COMSOL® model of a conductive hernia mesh. COMSOL®, a multiphysics finite element analysis software, was used to model the conductive electrode, determine voltage inputs and their resulting electric fields, and to test designs for creating a clinically relevant electric field stimulation within the proliferation range for fibroblasts. The model shows an electrically stimulated hernia mesh devised from the current methods of implanted polypropylene (PP) hernia mesh, by overlaying a thin gold surface onto the polymer

mesh, which is proposed to be connected to a small piezoelectric device. For maximized area of stimulation, one of the electrode connection points is insulated from the body environment to conduct the positive and negative electrode points to opposite sides of the wound, creating an electric field across the wound site. Electrode materials for the mesh conductance layer were tested within the model, which showed similar electric fields for each material. The small differences were shown to be based on the material properties, which allowed higher or lower conductance through the surrounding solution, phosphate buffered saline. Gold was chosen to be the conductive metal based on its moderate electric field and biocompatibility. A range of possible output voltages from the piezoelectric device were also modeled in a voltage sweep to show the maximum and minimum electric fields the tissues would experience within the previously set range. When several set points in the electric field were measured at a value of V_{in}=100 mV, the electric field average was 5.93 ± 1.24. The overall electric field showed maximum values at the anode and cathode, but there was also stimulation midway between the nodes that could supply moderate stimulation to cells wherever they may lie within the electric field. It was concluded from these computations that a voltage of 20mV – 250mV should allow for increased tissue healing through cellular proliferation when connected to gold coated polypropylene hernia mesh.

3.2 Introduction

3.2.1 Simple Hernias

For most of the population in the United States, hernias are a very common occurrence. There are multiple kinds of hernia and over a million people in the United States experience a hernia every year [8,9]. An abdominal hernia occurs when internal tissues protrude through a tear in the muscle wall lining the abdominal cavity (Figure 3) [2]. This tear, if left untreated, would

allow protruding tissues to enter foreign regions where they do not belong, which can ultimately result in bowel blockage and infection from intestinal tears or tissue necrosis [10]. Hernia surgeries, compared to other elective surgeries, are a relatively easy procedure. A few well-placed sutures to bring the abdominal wall back together patches the tear, but the original cause of the tear (weakened tissues) is still present and likely to be strained and tear again. By herniating, the wound location has further weakened the tissues and recurrence of the hernia is more likely. To prevent re-tearing of the hernia site, polymer meshes were developed to be placed across the weakened site to support the tissues. While mesh is mostly effective and has reduced recurrence rates from 63% to < 32%, comorbidities contribute to those number of patients who still experience a recurrence [1,11-13]. To mediate the factors (i.e. aging, lifting, obesity, weakened tissues) causing recurrence, regenerative medicine practices can be incorporated.

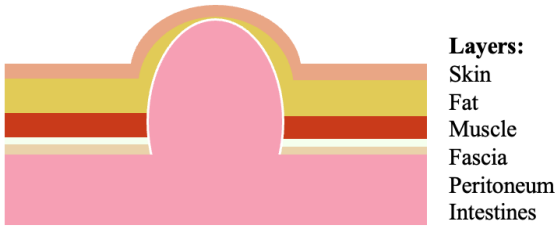

Figure 3. Diagram general abdominal hernia prolapse.

3.2.2 Electric Field Stimulation

Regenerative medicine is a newer area of biotechnology that incorporates engineering, tissues, material science, and medicine [4]. There are three main elements that are required for regenerative medicine to work: seed cell, scaffold, and stimulating factor [14]. In hernia repair, the seed cells are provided by the tissues and the scaffold/supportive material is the polymer

mesh and the natural extra cellular matrix the cells make. The stimulating factor in this research is an electric field. In general, exogenous (external) electrical stimulation utilizes the fact that wounded tissues have an endogenous (internal) electric field that promotes healing. Thrivikraman et al. (2017) notes that dermal tissues have an endogenous electric field (EF) of 100-200 mV/mm [5]. This EF stimulates the cells around the wound to proliferate and knit the region back together through electrotaxis, the direction of cellular movement [15]. Electrotaxis in a direct current (DC) would attract cells to the anode or cathode, depending on voltage amplitude and cell type, which can be utilized in moving cells more quickly towards a wound. Since AC current oscillates where the anode to cathode are located in proximity to the wound, the cells would remain in their original location and proliferate to strengthen the region [15]. Chen et al. (2019) found that higher intensities of AC < 100 V/cm (10,000 mV/mm) can be used to stimulate cell proliferation without cell death, but only for short time periods (< 1 ms) [4]. However, large voltages are unnecessary to achieve positive proliferation results and can instead be detrimental, leading to cell death [4]. A safe range of electric field for cellular proliferation should be determined based on the target tissues and the cells typically found in the region.

3.2.3 Soft Tissue Healing

For hernias found in the abdominal region, soft tissues are the general tissue type in which the hernia wound occur. The tissue layers consist of skin, fat, muscle, fascia, and peritoneum which all, when wounded, require new extra cellular matrices (ECM) to bridge across the injury and to provide the structure on which the main tissue cells will attach as they integrate. Fibroblasts are one cell type common to all these tissues, since fibroblasts are the main cell that creates new ECM when tissues are damaged [16,17]. In addition, Buckley (2021) shows how fibroblasts have been found to differentiate into new muscle cells and Mendias (2017) states

that fibroblasts guide skeletal muscle stem cells (satellite cells) to muscle wounds [18,19]. Furthermore, induced pluripotent stem cells (iPSC) can also be derived from fibroblasts to be used in repair of specific regions and tissue types [20]. For the purposes of this study, the further reduction of recurrence is the goal. Most hernia wounds repaired by hernioplasty fully recover after three months but only regain up to 80% of their original tensile strength [21]. Without a 100% restoration, recurrence is possible. Fibroblasts produce the materials that make up the ECM that contribute to this tissue strength. Kendall and Feghali-Bostwick (2014) notes that collagen type 1 is one fiber in the ECM that gives tensile strength, while elastin's crosslinked network allows the tissues to retain their elastic capabilities [22]. So, while studies on electrical stimulation of fibroblasts have not yet shown to what degree the specific proteins in the ECM are made when fibroblasts are stimulated, it can at least be seen that the fibroblasts proliferation and general ECM creation could be a factor for increasing the strength in the tissue region around the hernia site. Considering these factors and how fibroblasts are the main cell type that allows for the creation of new ECM, they will serve as the target cell line for proliferation and hernia tissue strengthening in this study.

3.2.4 Frequency and Electric Field Range

As previously noted, each cell type has a range of electric fields that the cell responds to and can proliferate within, before the voltage reaches a point where the cells are killed from the intensity. This research model will utilize an AC stimulation voltage, which is the model frequency's amplitude, from a small piezoelectric device previously studied by Norman (2021). The frequency will be set to 1MHz due to the frequency being within the therapeutic ultrasound range of 0.75-3 MHz [23]. Furthermore, Speed et al. (2001) found that a medically safe

frequency of 1MHz stimulates soft tissues at a depth of 3-5 cm, which is approximately the depth of many patients' hernias [24].

The electric field range for the fibroblast proliferation is based on current literature findings from multiple studies. Chen et al. (2019) found that an AC frequency of 1 Hz and an electric field between 65-200 mV/mm promoted cellular proliferation in iPSC [4]. Bhang et al. (2016) found that an AC frequency of 0.5 Hz and a wave amplitude of 900 mV increased fibroblast proliferation and differentiation to myofibroblasts for dermal wound healing, but the electric field was not noted [3]. While each study considered has its own unique methods and results, this research model took the literature into consideration and will be using an approximate EF range for fibroblast proliferation of 20-300 mV/mm.

3.2.5 Surgical Application

Each patient and hernia is unique, and the type and size of hernia mesh required varies with each unique case. The method of implantation also varies based on the surgeon's skill level and previous experiences. One thing that is consistent for all hernioplasty procedures, however, is that the hernia mesh should be easy to handle during implantation and uniform in structure to allow for cutting to suit the patient's specific hernia [25]. To allow for cutting, commercial polymer meshes utilize a specific weave pattern called a warp knit that does not unravel when cut. The knit also gives the mesh a soft and flexible feel that can not only match the human body movement, but also gives the mesh design good tensile strength and elasticity (Figure 4) [26-29].

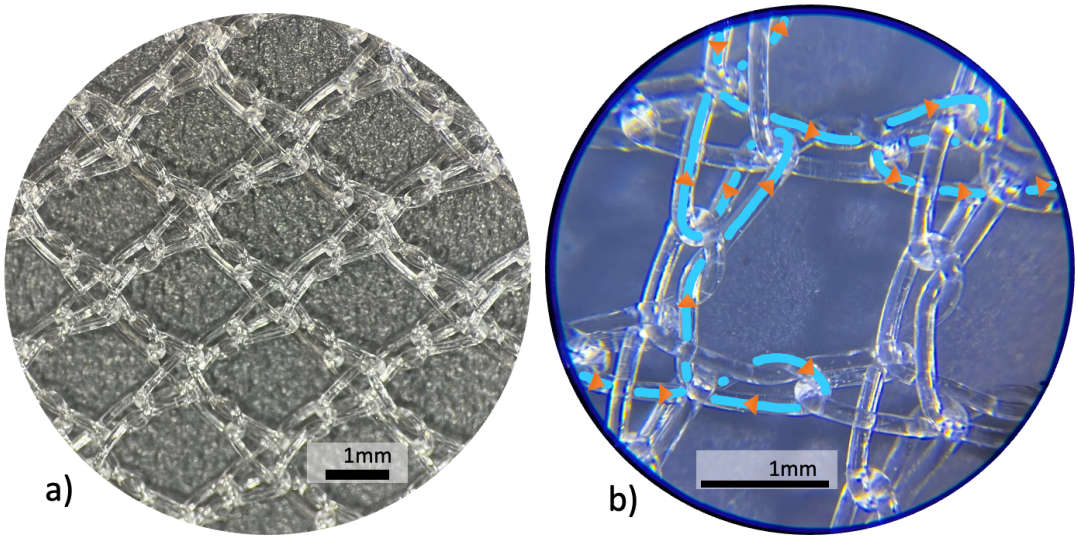

Figure 4. Image **a)** of uncoated polypropylene mesh and close schematic **b)** of warp knitted pattern found in PPKM505 58 GSM from Surgical Mesh™ Division Textile Development Associates, Inc.

For the creation of a conductive mesh that allows for hernia electrical stimulation, a thin layer of conductive metal would be layered onto the polymer mesh surface. As Figure 2 clearly displays, the mesh is comprised of monofilaments woven to create a porous and flexible network, which can be difficult to model. An idealized model is used in which each group of monofilaments is assumed to be one larger woven unit fiber with a combined width, and each intersection point of fibers would conduct the connected circuit to the next fiber section. The immediate aim of this study is to create a mesh electrode model that can be used to determine expected values of EF in a conductive mesh design for fibroblast proliferation around and in contact with the mesh to strengthen the hernia region.

3.2.6 Model Design

The electrode model, in which polymer mesh is represented by a solid fiber and has a layer of conductive metal adhered to the surface, can be designed in a single "unit" method where only a small section of mesh is modeled and analyzed to then be expanded for an overall product concept (Figure 5). Each unit should connect to the next, but a final product, if produced, would implement this design in large scale production of mesh. First, the conductive layer must be able to be continuous for proper electric field conduction. In addition, a connection point for the piezoelectric voltage input would be incorporated into the design to limit difficulty of use by surgeons and to ensure the hernia region receives electrical stimulation throughout the hernia region. Furthermore, the unit model should be able to be expanded into a larger mesh product that could be used for delivering an electric field to the hernia region. Before this electrically conductive mesh can be implemented, a computational study of the model will determine the idealized design of the electrode, the range of input voltages that could be expected for the desired EF values for fibroblast proliferation, and the conductive metal material that provides a desirable EF when stimulated.

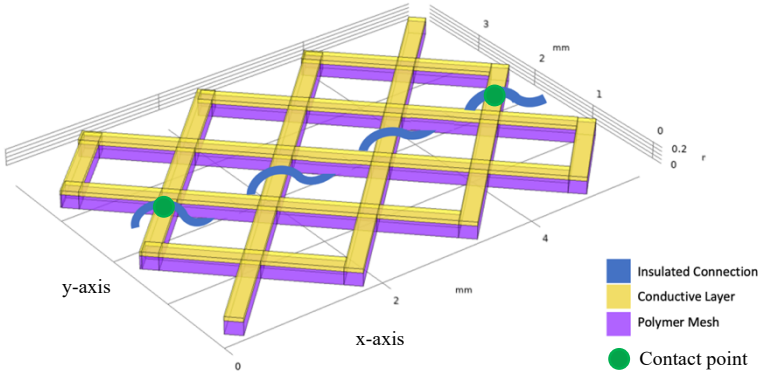

Figure 5. Unit design of idealized conductive hernia mesh in COMSOL® where the insulated voltage input connection point is woven through the mesh.

3.3 Materials and Methods

3.3.1 Study Parameters

Since the previous work leading to this study used AC current, this computational model using COMSOL® was time dependent and used a frequency of 1 MHz to stimulate the model as would be expected for ultrasound waves *in vitro* from the previous research conducted by Norman (2021), who measured maximum voltage amplitudes of 20-28 mV from a single lead zirconate titanate piezoelectric disc (Figure 6) [23]. The time points viewed for the results covered half of one wave ($2.5x10^{-7}$ – $7.5x10^{-7}$s) at an increment/step of $0.1x10^{-7}$s. Measurements of the EF and conductance can then be taken at any time point/step along the section of frequency wave range being analyzed. For the purposes of this study, the maximum EF at the wave peak will be the focus to gauge cellular viability at the highest voltage expected. Furthermore, the EF and conductance measurements were taken close to the mesh conductive surface in PBS solution (Z-axis plane: 0.21mm) where the EF should be highest and where the cells would be in contact with the mesh. Measurements taken at the center of a mesh pore was done to avoid measuring EF within the modeled mesh material, but more importantly to find the expected EF range a fibroblast cell may experience when not in direct contact with the mesh.

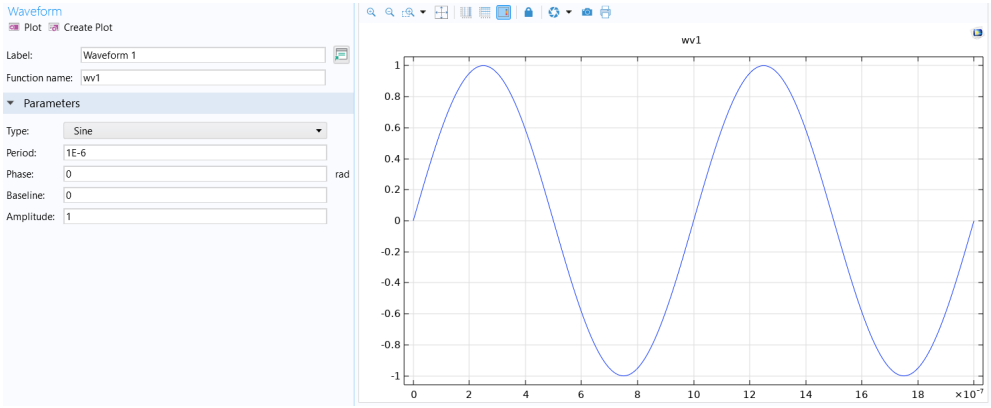

Figure 6: Frequency (1E-6) and voltage amplitude (1V) used in this snapshot of COMSOL® modeling parameters.

3.3.1.1 Electric Field Equations

Electric field (E) can be calculated by a simple equation that looks at the source charge (Q) and the distance to the measurement point (d), plus Coulomb's constant (k).

$$E = \frac{k \cdot Q}{d^2}$$

This equation does not take into consideration material properties, though. To calculate the EF within the model, COMSOL uses Gauss' law, which states the "electric flux through any closed surface is proportional to the total electric charge enclosed by this surface" [30]. More importantly, Gauss' Law allows for material properties to be considered in the electric field calculation and not only charge and distance. The general Gauss' law formula is as follows, where ∇ is the electric flux or gradient and V is the electric potential.

$$E = -\nabla V$$

The material property of dielectric constant comes into play when Gauss' law is represented by this secondary equation:

$$\varphi E_0 dS = \frac{q}{\varepsilon_0} \quad (1)$$

where φ represents electric flux through the surface, E_0 represents the external electric field, dS is an infinitesimally small vector perpendicular to the surface that the flux is being measured through, q is the charge, and ε_0 is the permittivity of free space. Then, assuming E_0 and dS are constant over the Gaussian surface,

$$E_0 A = \frac{q}{\varepsilon_0 A} \quad (2)$$

where A is the area of the charged surface. The material dielectric constant (K) is then added to the space between the charges, where the material charges (±q') and the outside charges free charges (±q) create the electric field.

$$\frac{E_0}{E} = K \quad (3) \qquad E = \frac{q-q'}{\varepsilon_0 A} \quad (4) \qquad \varphi EdS = \frac{q-q'}{\varepsilon_0} \quad (5)$$

Equation 2 and 3 can then be combined to create equation 6, and equations 4 and 6 combine to become equation 7.

$$E = \frac{q}{\varepsilon_0 KA} \quad (6) \qquad \frac{q}{K} = q - q' \quad (7)$$

Equations 5 and 7 then combine to create the final Gauss equation:

$$\varphi EdS = \frac{q}{\varepsilon_0 K}$$

which shows how to material dielectric constant (K) is used in calculating the electric field in COMSOL [31-33].

3.3.2 Materials

The materials used for this study are the same as what would be expected in a hernia repair mesh. Since the long-term goal of this model is to be a medical device product, all materials should foremost be biocompatible. Polypropylene (PP) hernia mesh was chosen for use in this model due to the many desirable qualities that contribute to its comparable success. Not only is PP inexpensive and easy to make, but it is also hydrophobic/non-polar, which aids in preventing tissue adherence and strain on the healing wound [9]. PP also has a high heat resistance to allow sterilization without compromising the mechanical properties' integrity, flexibility, or the overall rigidity that makes handling easier during surgery [23,26,34]. Most importantly, however, is the attribute of non-toxicity to the tissues, as it becomes integrated into the body [26].

Silicone rubber, utilized as an electrical insulator in this model, is a material that is considered bioinert and non-toxic [35]. Silicone is often used as an insulator for electrical circuits, which would protect this circuit model from shorting inside the body and would also not agitate the tissues [36,37]. Another component in the model, gold, is also highly biocompatible and bioinert and is often used in electrodes that interface with cells and live tissues [38]. Most metallic materials oxidize easily and corrode due to fouling and body fluids [4]. In the event of corrosion or oxidation of the metal surface, gold ions and larger nanoparticles have shown to be non-toxic in *in vitro* and *in vivo* applications [39,40].

The last material is essential, since the body is dynamic, and a model of an *in vitro* device requires a solution or body fluid mimic that can show similar reactions to the effect being tested. This *in vitro* computation model utilizes PBS (phosphate buffered saline), a saline balanced solution, to test and visualize the electric field and serves as the outer boundary of the model for viewing the EF (Figure 7).

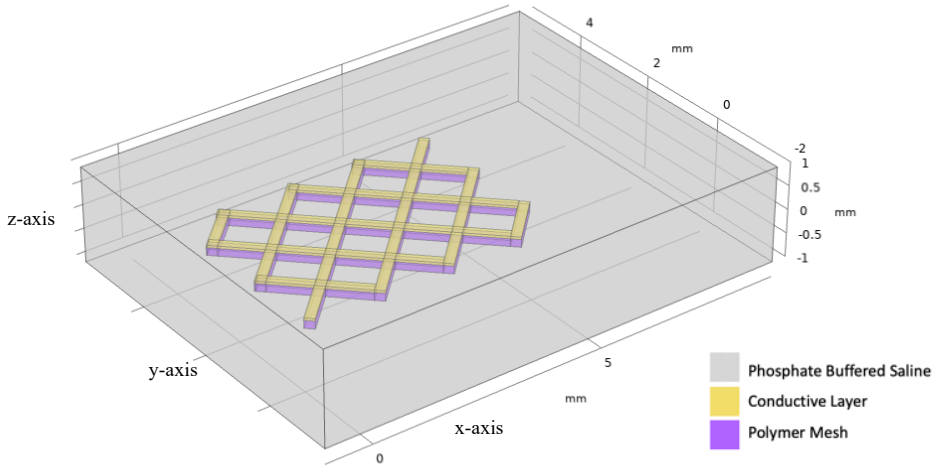

Figure 7. 3D model of idealized unit cell conductive mesh electrode surrounded by PBS.

The model and study were designed to show the expected EF in three dimensions for one small unit of the hernia mesh electrode. Hernia repair mesh, which has woven monofilaments of 0.0125mm diameter, was represented by a polypropylene material of solid fibers whose width and thickness were 0.2mm to represent a solid woven thickness. The mesh woven diamond pattern has a pore width of 1.5mm to approximate the woven mesh pore size of 1.5x1.3 mm (PPKM505 58 GSM from Surgical Mesh™ Division Textile Development Associates, Inc). This mesh pore size being >1mm is beneficial for preventing granulomas and inflammation around the hernia repair site [1,26,41]. The layer of conductive metal of 0.02mm was then added to the upward facing surface of the larger polypropylene fibers. Due to COMSOL® minimum finite element analysis (FEA) limitations for the computation, any given element cannot be smaller than 548nm. Even if an element is above this minimum, design and study parameters can create warning and error messages. Therefore, to avoid these issues, the design used 0.02mm for the conductive metal coating thickness with the knowledge that a practical model would have a much thinner metal layer in the nanometer range.

3.3.3 Conductive Material Comparison

One of the goals of modeling the electrode is to determine the expected electric field output from an idealized electrode prior to an *in vitro* test to ensure optimal ranges of electric field for cellular stimulation. COMSOL®, a multiphysics computational software, was chosen due to its capabilities for modeling AC currents at high frequencies across three dimensional structures with an unlimited number of materials. While polypropylene holds a small capacity for electrical conductance, it is not enough to be considered a conductor. A highly conductive metal material was added to the model mesh surface. This thin layer not only facilitates the conductance, but also completes the circuit to the current source: the piezoelectric device.

To verify the electric field expected across a conductive polypropylene hernia mesh, common conductive biomimetic and electrode materials were modeled to compare with each other (Table 1). The modeling of the conductive metals also served to identify the idealized material to use as the conductive layer for continued testing of EF within the model. Each conductive material tested in the COMSOL® model was run with the same study parameters with a frequency of 1 MHz and a wave amplitude (voltage input) of 100mV. The results of the EF were visualized on the same mV/mm color scale, limited from 0 to 20 mV/mm. The material properties of importance for the electric field modeling were relative permittivity (dielectric constant) and conductance. All materials not already in the COMSOL® database were input manually with their properties.

Table 1: COMSOL® Model Material Properties

Material	Electrical Conductivity (S/m)	Relative Permittivity (unitless)
PBS (1x) [42-44]	1.20	80.0
Silicon [45,46]	3.16E-12	4.00
Polypropylene [47,48]	6.25E-15	2.10
Titanium [49]	7.41E5	1.00
Copper [49]	6.00E7	1.00
Gold [49,50]	4.42E7	6.90
Platinum [49,51]	9.43E6	7.50

3.3.4 Anode and Cathode Placement

In determining the final model set up, the placement of the anode and cathode was studied to later justify connections and the piezoelectric device placement *in vivo*. This was done by selection of three different spacings between the anode and cathode (Figure 8). The EF and surface conductivity for each spacing was visualized.

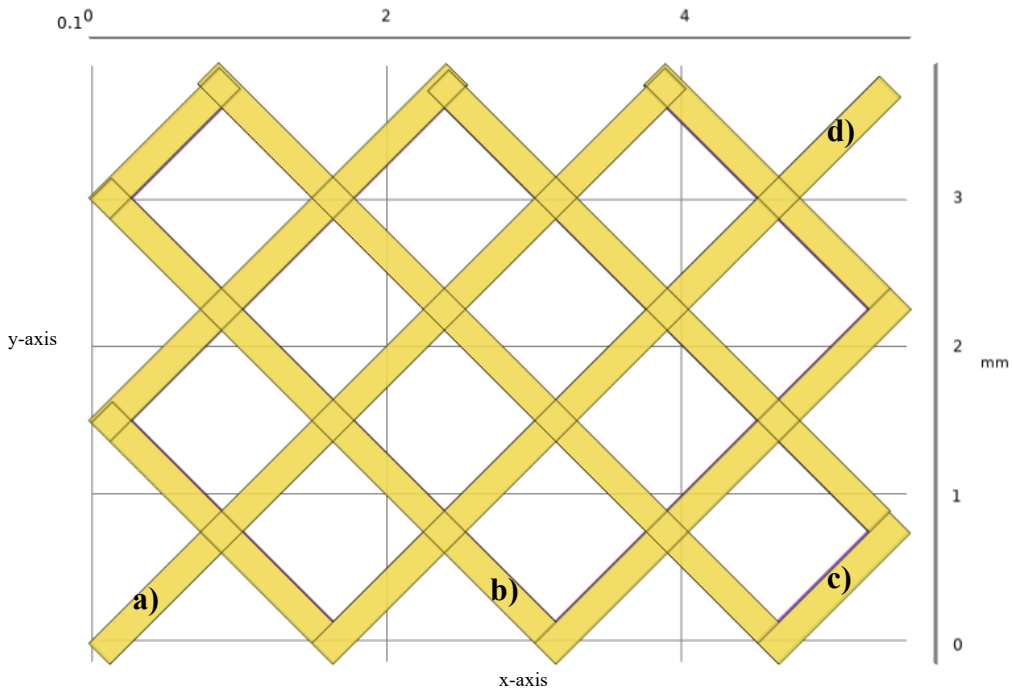

Figure 8. a) The location of the anode, the possible locations for the **b)** cathode at 1 pore away, **c)** cathode at 3 pores away, and **c)** cathode at 4 pores away within the unit model.

3.3.5 Clinical Relevance of Model

To maximizing the electric field area for cellular stimulation, the anode and cathode of the electrode should be on opposite sides of the mesh. This can easily be done *in vitro* by connecting the piezoelectric device to opposite ends of the conductive mesh surface. However, this is not the best design for an *in vivo* application since long wires would agitate the wound and be difficult to handle in surgery (Figure 9). To mitigate these issues, the use of an insulated wire, or "electrode extender", woven through the mesh as one connection point for the device would allow the electrode to conduct the current to the opposite side of the mesh without being exposed to solution *in vitro* or tissues *in vivo* prematurely. The positive and negative electrodes on opposite sides would maximize the area around the wound that can receive stimulation, and the

metal electrode layer would conduct the current from the anode/cathode back to the piezoelectric device to complete the circuit. Silicone, a biocompatible and non-conductive material, was chosen to be the insulator around the conductive electrode extending wire to be woven across the mesh. The mesh electrode should experience the EF in the same way, regardless of whether the anode and cathode are connected by use of a woven insulated wire, or if the connection is made by looping the connector around.

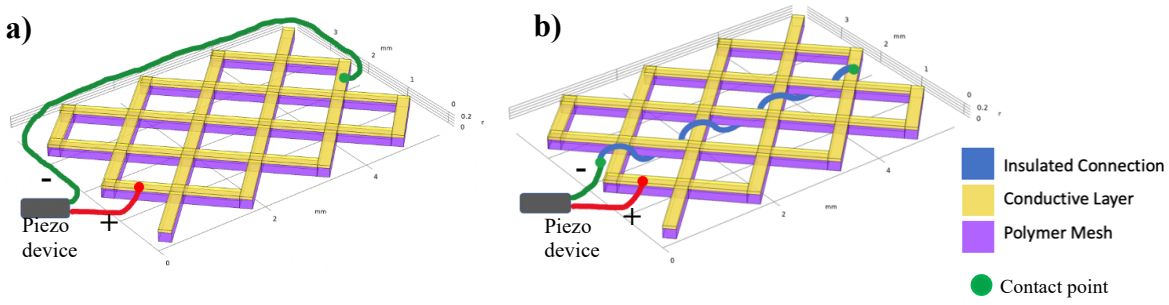

Figure 9. Idealized unit cell diagram of possible piezoelectric connection to maximize EF where **a)** uses a short cathode (red) and a long anode (green) wire connection to loop around to a connection point and **b)** utilizes a short cathode (red) and a close insulated connection point that extends the anode (green) across the mesh area. Both red and green wires are insulated.

3.3.6 Silicone Insulated Connection

The unit model was expanded to include the insulated wire for the piezoelectric device to connect to (Figure 10). Since silicone is an insulator and the final proposed unit model design incorporates an insulated conduction wire that would extend the piezoelectric device anode for maximized area of stimulation, the unit model with and without the insulated wire was compared.

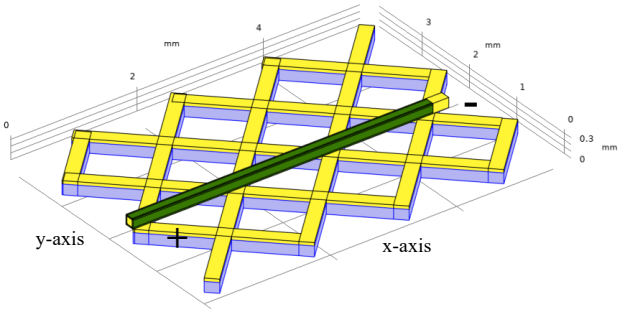

Figure 10. Idealized unit model utilizing insulated wire (green) for connection to voltage source (piezoelectric device). The left (x=0) end of the insulated wire is not shown to be in contact with the mesh surface since the piezoelectric device would connect to the insulated wire at this location.

3.3.7 Area of Electric Field

To test how the electric field propagates throughout the area of the modeled unit cell mesh, the electric field values were checked at various distances across the mesh area between anode and cathode in the COMSOL® 3D model, with each specific measurement location being in the center of the pore and on the z-axis plane of 0.21mm just above the mesh surface (Figure 11). As mentioned previously, maximum EFs will be reported wherever they exist. For cellular stimulation, a moderate EF is necessary to ensure cell death due to high voltage is mitigated and all cells are stimulated within a safe range for proliferation.

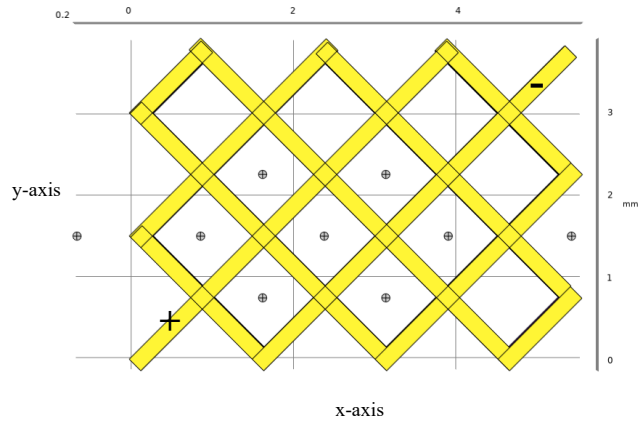

Figure 11. Electric field: XY-Axis points at indicated locations in 3D COMSOL® model where electric field values were checked in pore centers on the z-axis plane (Z=0.21mm).

3.4 Results

3.4.1 Study Parameters

In this time dependent study, the flow of the frequency wave across the electrode surface was a factor that needed to be considered to verify that a given point in the electric field showed the correct value for that time point. A full peak to peak wave with time point increments of 0.1s was checked for lag (phase shift). It was determined that the phase shift was present but negligible in value and <1 mV for all time points.

3.4.1.1 Effect of DC in Model

Another parameter that needed verifying was DC verses AC stimulation. Due to the maximum EF occurring at the peak amplitude in the frequency within the AC time dependent study, a comparison of DC to AC showed AC to have similar EF when the same model was run with a DC stimulation that is not time dependent (Figure 12). The results would not be identical, however, because the nature of AC and DC serve very different purposes. DC creates a steady state of constant voltage being delivered, while AC oscillates the voltage output over time, creating its frequency nature. Weststrate et al. (2010) found in testing and their COMSOL® modeling that this AC oscillation can create currents and voltages within other conductive materials around it [52,53]. Since this study is designed to show a maximum EF range across a conductive hernia mesh, it is possible the difference in maximum EF between the DC and AC model comparisons is due to the AC capabilities that DC does not have. Within the COMSOL® modeling software, a frequency domain can also be used instead of the typical time domain for AC. A frequency domain finds solutions at an angle instead of a time point, based on the Fourier transform equations use of harmonics and angular frequency [54]. Since the frequency domain was not utilized in this study, it will be considered for future modeling.

The time dependent AC modeling used in this study shows what is, for all intents and purposes, a snapshot of similar results a DC model would show. This is because the timepoints within the AC model were chosen to be at the times when the frequency would have the maximum amplitude to know the model's maximum expected EF (Figure 12). Since steady state DC is equivalent to the V_{RMS} in an AC circuit, it is reasonable to see lower overall EF from a DC study [55]. For this model, the further effect of DC on hernia tissues will not be considered in the study scope.

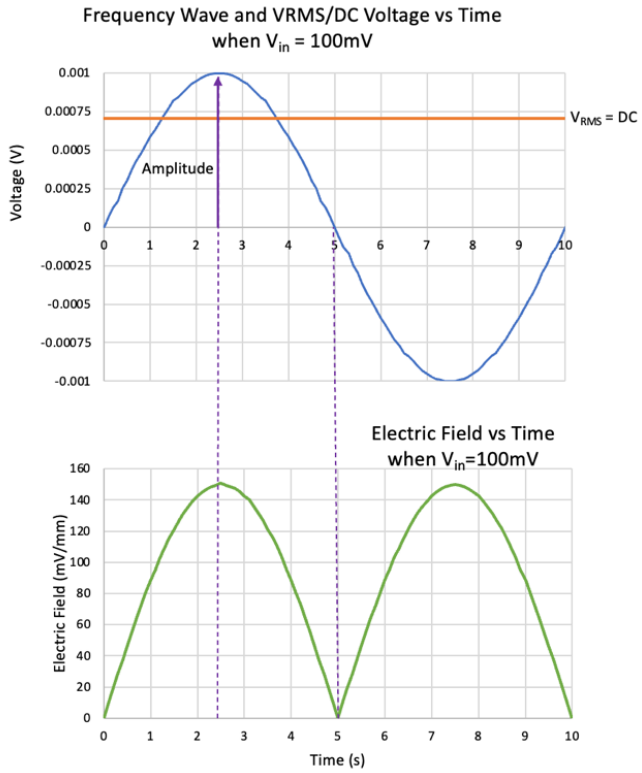

Figure 12. Comparison of **a)** AC and DC current where V_{in}=100mV and **b)** expected EF at the wave timepoints. Shows positive EF maximums occur at +/- frequency peaks.

3.4.2 Conductive Material

For material comparisons, the idealized metal to coat the mesh (given biocompatibility and non-toxicity and ability to create the targeted range of electric field) was gold (Figure 13). Each material's maximum EF occurred at the anode and cathode locations. And when V_{in} = 100mV, the maximum EFs were 140, 131, 101, and 101 mV/mm for platinum, gold,

titanium, and copper, respectively. While the disparity from 101mV/mm to 140 mV/mm is large, it is not a clinically relevant condition for the end goal of this model. The model input can be specified for the material. The relative permittivity of the materials was the greatest contributing factor in how strong the EF was through the PBS solution, given the voltage input was the same for all the materials tested.

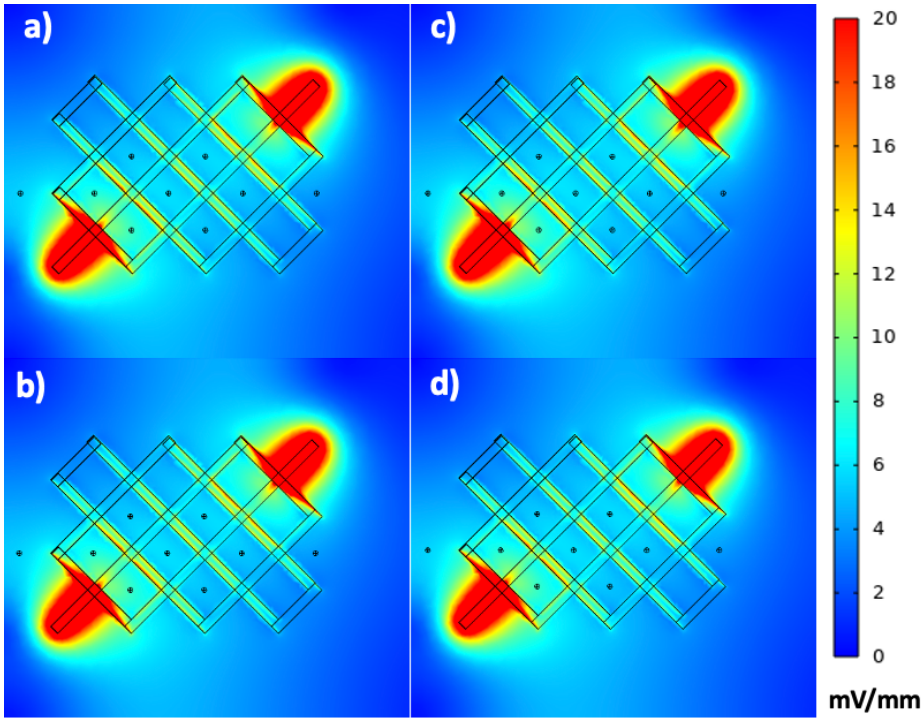

Figure 13. Electric field comparison of materials **a)** Copper, **b)** Titanium, **c)** Gold, **d)** Platinum where EF color ranges from 0-20mV/mm when V_{in} = 100 mV.

3.4.3 Anode and Cathode Placement

The anode and cathode visualization of current and electric field shows that not only does current follow the path of least resistance between nodes, but the electric field spreads across less of the electrode area as the cathode and anode are placed closer together (Figure 14). Less area of stimulation could produce less cellular proliferation in the surrounding fibroblast cells.

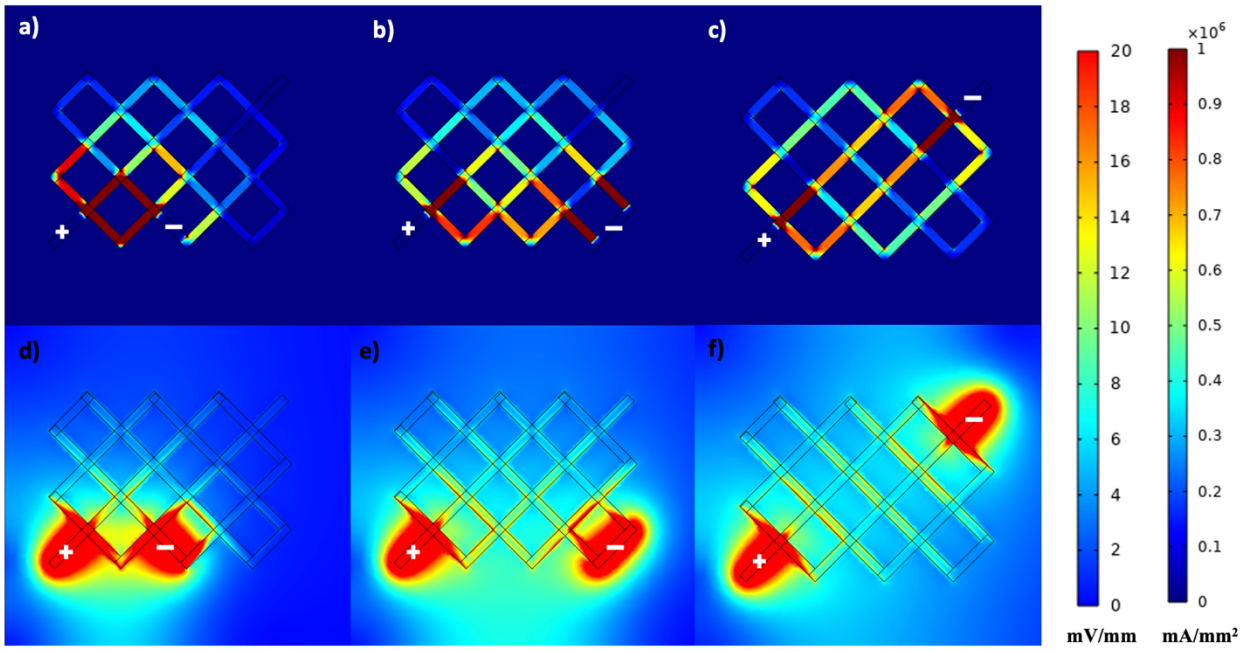

Figure 14. a,b,c) Current density over color range 0-1.0E6 (mA/mm^2) and **d,e,f)** EF over color range 0-20 (mV/mm) in PBS solution as electrodes are increasing in distance apart. V_{in} = 100mV

3.4.4 Voltage Input Sweep

Based on the previously proposed range of electric fields for fibroblast stimulation and the noted distance in spacing of anode and cathode for the largest area of EF, this model's electric field output indicates an input voltage between 20-250 mV would produce an electric field of approximately 20-300 mV/mm (Table 2).

Table 2. V_{in} Electric field sweep using gold conductive metal on PP mesh modeled in COMSOL®.

Voltage$_{in}$ (mV)	**Middle Area EF* (mV/mm)**	**Max EF** (mV/mm)**
1	0.0438	1.31
10	0.438	13.1
15	0.623	19.6
20	0.876	**26.2**
100	4.38	**131**
150	6.57	**197**
250	11.0	**328**
300	13.1	393
500	21.9	655
1000	43.8	1310

*Middle Area EF: point midway across mesh located at (2.38, 1.5) with moderate/low EF
**Maximums occurring at anode and cathode

3.4.5 Area of Electric Field

With gold selected as the material for the electrode modeling, the voltage input sweep showed moderate electric field values across the mesh and PBS when electric field values were quantified (Table 2). The maximum EF can be seen to occur at the anode and cathode points, with lower but relevant EFs midway across. (Figure 15).

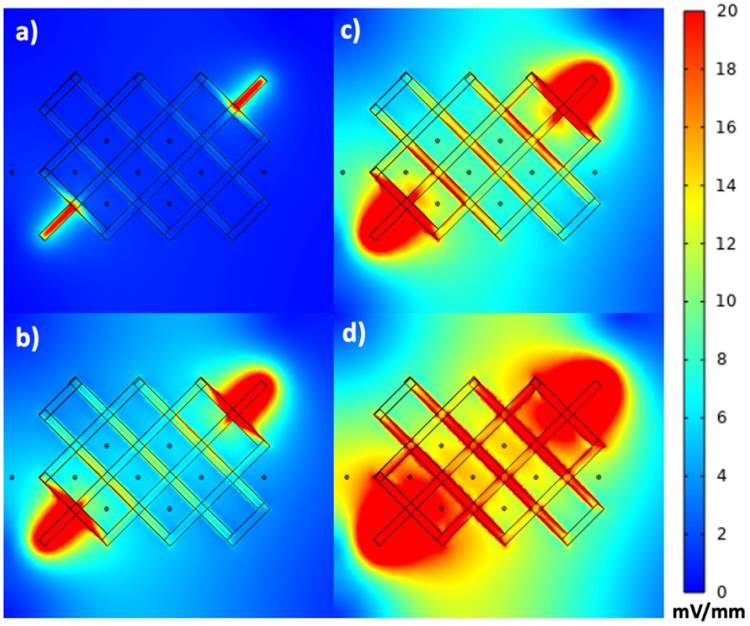

Figure 15. Visualized EF based on increasing V_{in} **a**) 20mV **b)** 100mV **c)** 150mV **d)** 250mV where EF color ranges from 0-20 mV/mm

When the electric field was measured across several points located at the center of the mesh pores in PBS solution (Figure 11), the maximum EF was 8.16 mV/mm and the minimum value was 4.18 mV/mm, with an average across all the points of 5.93 ± 1.24 mV/mm (Table 3). These values show that between the maximum EF locations at the anode and cathode, a moderate level of stimulation would occur across the mesh area for cellular proliferation. By using a wide distance between anode and cathode, the area of electric field stimulation is larger. While the model maximums occur at the anode/cathode, these lower values across the area between the

anode/cathode would still allow cells in the center of a mesh pore to be stimulated for proliferation.

Table 3. Electric field points at the center of pores across mesh area with V_{in}=100mV. Modeled with maximum distance separation of anode/cathode.

X-axis Point (mm)	Y-axis Point (mm)	EF (mV/mm)
-0.63	1.50	5.64
0.88	1.50	7.65
1.63	2.25	5.43
1.63	0.75	8.16
2.38	1.50	5.93
3.13	2.25	5.82
3.13	0.75	5.22
3.89	1.50	5.34
5.39	1.50	4.18
Average EF	5.93 ± 1.24	

With the model being in three dimensions, the EF area in the Z-axis component was also verified by measuring EF at two locations in PBS solution (Figure 16), which showed that as distance from the mesh conductive surface increased, electric field magnitude decreased (Table 4) (Figure 17). It was also observed that the EF magnitude reached higher values above the conductive layer in the model, whereas the EF below the conductive layer may have been obstructed by the non-conductive PP mesh. Three EF ranges (0-20, 0-50, and 0-300 mV/mm) are shown in Figure 18 for visualizing the EF at different clinically significant values (20-300 mV/mm) that this study has targeted for fibroblast stimulation. While the EF maximum in the XY plane for a voltage input of 100 mV was 131 mV/mm (Table 2), the EF maximum in the YZ plane for the same 100 mV input was 271 mV/mm. This maximum in the YZ plane is higher than the XY plane maximum, which should be taken into consideration for determining final voltage input values.

Table 4: Values of EF in the Z-axis plane. Measurements taken in increasing distances above the mesh surface located at Z=0.21mm			
X-Axis Location (mm)	**Y-Axis Location (mm)**	**Z-Axis Location (mm)**	**EF (mV/mm)**
Point 1: X,Y (0.6,0.453)			
0.600	0.453	0.214	67.3
0.600	0.453	0.279	57.0
0.600	0.453	0.356	39.8
0.600	0.453	0.527	20.1
Point 2: X,Y (2.35,1.50)			
2.35	1.50	0.218	16.3
2.35	1.50	0.277	16.4
2.35	1.50	0.354	16.4
2.35	1.50	0.526	15.9

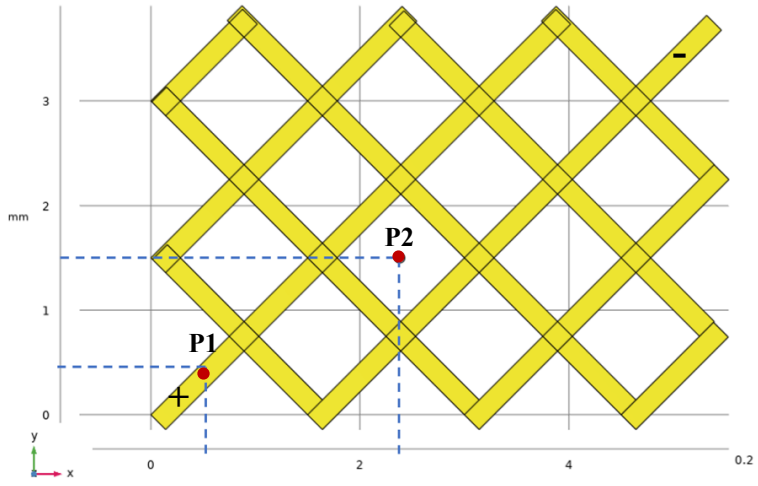

Figure 16. XY location where Z-axis EF was measured.

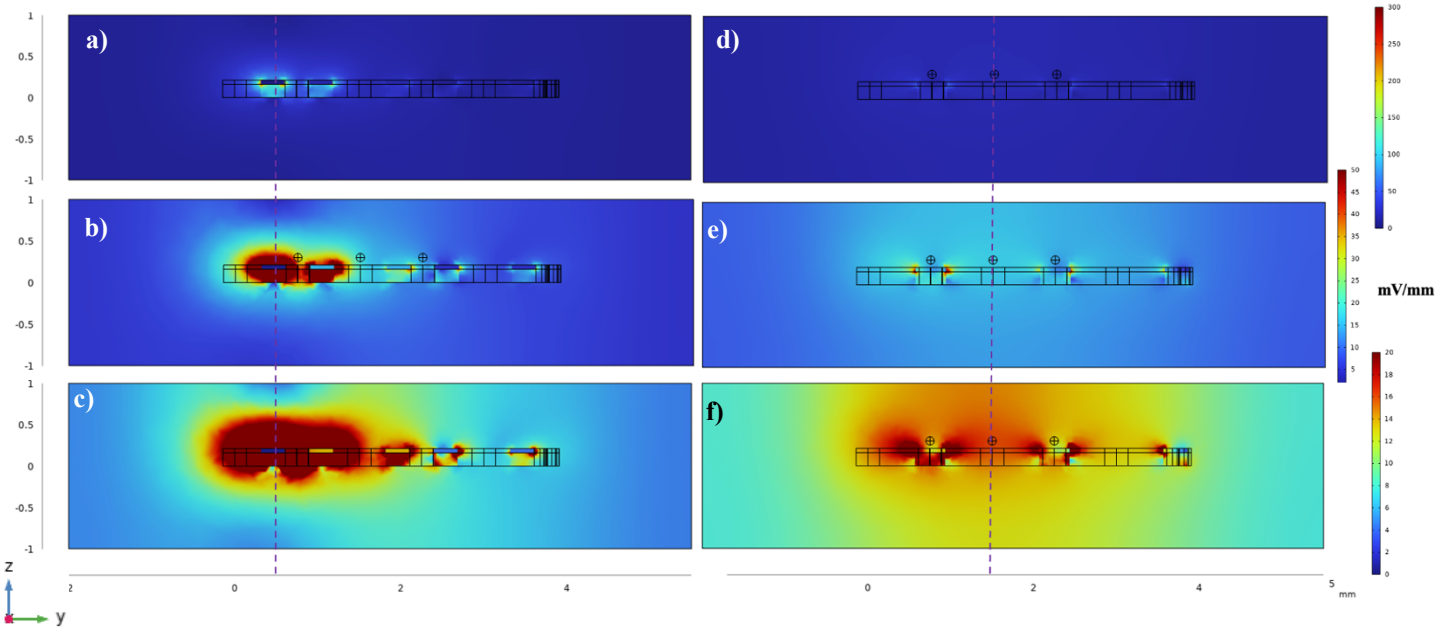

Figure 17. Z-axis area of EF which shows a quick decline in EF magnitude further from mesh surface and EF propagation at moderate levels within the 20-300 mV/mm stimulation range. **a,b,c)** Point 1 (P1) and **d,e,f)** Point 2 (P2) shows higher EF propagation above conductive layer than below (through PP mesh). Images **a) d)** were imaged on an EF color scale of 0-300mV/mm, while **b) d)** on a scale of 0-50mV/mm and **c) f)** on a scale of 0-20 mV/mm. V_{in}=100mV.

3.4.6 Insulated Unit Model

With the conductive material chosen, and the anode and cathode distances established, the final element that the future hernia mesh product required was the verification of similar EF when a conductive insulated wire is incorporated into the unit model. For all voltage intensities tested in the voltage sweep (Table 2), the same sweep was used where the anode and cathode were located at opposite ends of the insulated component, as expected in the future product. The insulated unit model showed consistently lower values of EF compared to the non-insulated idealized unit model. Figure 18 shows the two model's anode/cathode locations and visualized EF, and Figure 19 shows a linear increase in EF as V_{in} increases for both insulated and non-

insulated unit models. A linear trendline for EF measured midway across the insulated model area was also found, despite being much lower than the maximum EF at the anode/cathode. Both model's electric fields were created by a V_{in} = 100mV, where the non-insulated unit model had a maximum EF at the anode/cathode of 131 mV/mm and the insulated EF was 91.2 mV/mm. Not only does the insulated model show that a decent level of EF will still be propogated *in vitro*, but the full area across the mesh should also receive similar values of stimulation as the model without an insulated component in PBS solution. The linear trendline makes predicting EF values for future work more accurate to target the proposed fibroblast proliferation range.

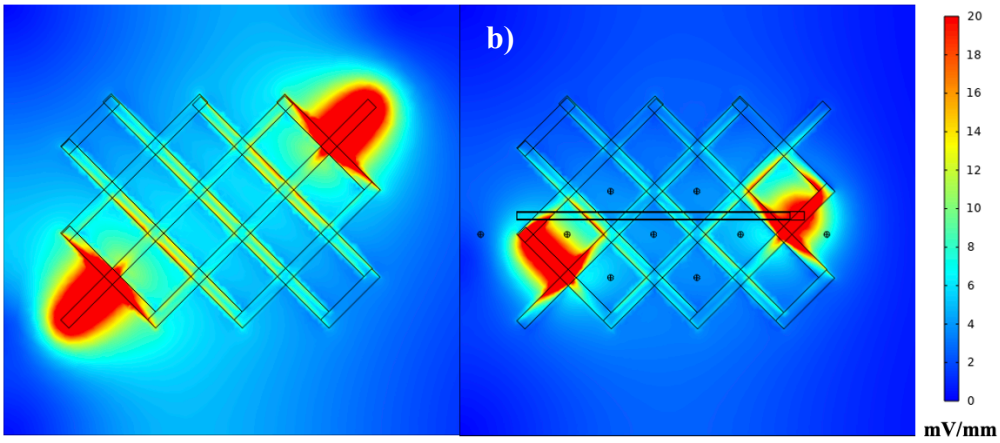

Figure 18. a) Non-insulated unit model anode/cathode locations and visualized EF and **b)** silicone insulated conductive wire unit model anode/cathode locations and visualized EF. Both models used V_{in} = 100mV and EF range of 0-20mV/mm.

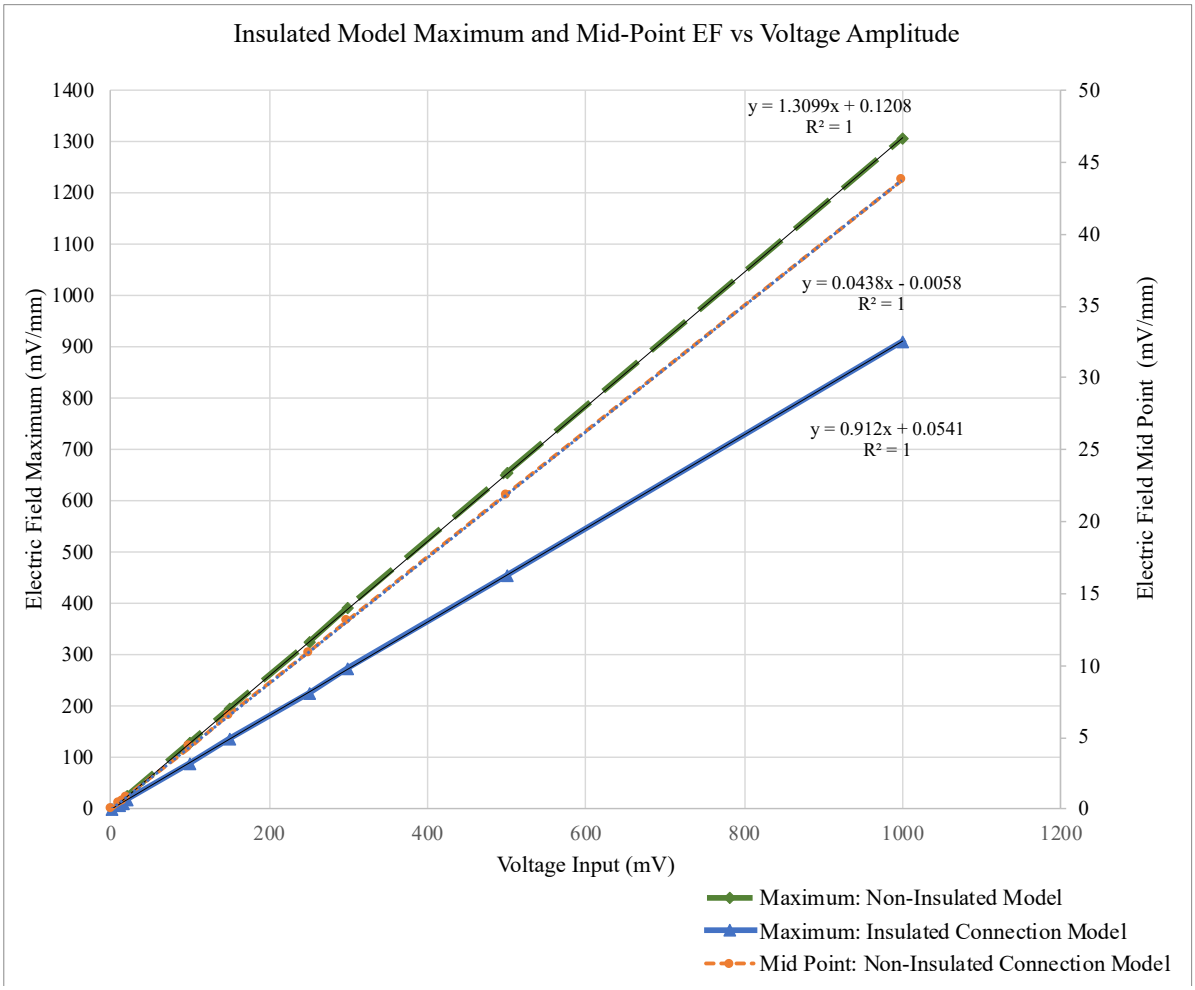

Figure 19. Comparison of electric field for an insulated unit model and an idealized unit model without an insulated component. Both show linear trendlines as V_{in} increases.

3.5 Discussion

Given that the goal of this study was to model a conductive hernia mesh that could aid in the future design of an electrically stimulated hernia mesh, the results gave insight into many faucets and possibilities of what could be done to achieve this later product.

All measurements of EF for the XY electric field propagation were taken at the Z-plane of 0.21mm, which is just above the mesh conductive surface in PBS solution in order to determine the maximum values the model produced around the mesh. This was done because, as

the distance from the mesh surface was increased, the EF decreased (Figure 17). Knowing the greatest predicted EF the future *in vitro* cells would experience, near or in direct contact with the mesh surface modeled in this study, could determine whether the cells are encouraged to proliferate or killed from high intensity EF instead.

The first consideration was the conductive material layer. While the selection of gold over its biocompatible partners (platinum and titanium) was simple for the purposes of the model, platinum or titanium could be a better material to use when this model is made into a product. Besides biocompatibility, the material choice is dictated by how manageable it is to obtain and how the metal coating on the mesh can be achieved. The product version of the chosen material may also be influenced by surgeons' preferences. Another major consideration on material options is the cost of the material. Platinum shares many of the same biocompatible properties as gold and could be a viable option for the metal electrode layer, but platinum can be more expensive than gold. Titanium on the other hand is much less expensive and still biocompatible, but it is also considerably less conductive than platinum or gold. The material ultimately chosen should enhance tissue strength in whatever capacity it can lend to hernia repair.

Another major consideration this study set to determine was the voltage amplitude for fibroblast cellular proliferation. Based on this study's computations on the unit model, an expected range of voltages were determined to be possible between a V_{in} of 20 and 250 mV. This approximate voltage range is predicted within the unit model to be able to create a maximum EF at the anode/cathode points of 26.2-328 mV/mm (Table 2). The verification of this EF range is important to ensure tissues would not be subjected to stimulation that may harm the fibroblasts.

The range predicted for fibroblast proliferation based on recent research publications should be further refined through continued literature review and *in vitro* studies [3,4,18-20].

For the placement of the anode and cathode, the model showed that the further the anode and cathode were from each other on the unit model, the more area around the electrode mesh would be stimulated from the induced electric field. Placing the anode/cathode closer together provided a more concentrated electric field for the area directly between them. While this closer proximity may be beneficial in some studies, the general goal for this electrically active hernia mesh is to stimulate the whole region surrounding the hernia wound to strengthen the tissues. There may also be some benefit in aligning the anode and cathode across the hernia wound for cells to be stimulated as close to the wound as possible. Wounds naturally have the endogenous EF to guide cells to the wound, but the AC stimulation has not shown to directly pull cells towards any direction [6]. Regarding the area of stimulation, the voltage sweep and points at pore centers measuring EF showed that not only were large regions of the model able to be stimulated from two points (anode/cathode) some distance apart, but even in the lowest EF region, there was still moderate EF values that would aid in cellular proliferation in a product application of this model. As stated previously, the measurements for EF across the mesh's area were place in the center of pores to measure the EF level a cell not in contact with the mesh would experience. Cellular proliferation through direct contact with current is not within the scope of this study.

The product application unit model incorporated the insulated wire for electrode extension. Using the furthest anode/cathode placement at opposite ends of insulated wire, the insulated unit model showed lower EF values than its counterpart that had the anode/cathode at the maximum corners of the idealized unit model (Figure 18). Despite this, the EF values from

the insulated unit model were not significantly lower than its comparator and cellular stimulation would still be very possible. The lower EF is possibly due to the smaller distance between the anode and cathode. The proposed unit model design, using the insulated connection point, did allow the electric field to expand across the electrode area without the use of long wires (Figure 9). This creates a promising set up for the piezoelectric device to connect to the conductive mesh without compromising stimulation of the maximum area possible.

Considering these results, this model and product design, when physically produced, should allow surgeons to cut the sputter coated hernia mesh wherever they desire. Multiple insulated connection points would be needed at intervals parallel to each other across the mesh piece to accommodate mass production of hernia mesh (Figure 21). These parallel insulated connection points should not modify the current mesh preparation and procedure significantly. The surgical instructions would be minimal and cover how to connect the piezoelectric current source to maximize the area of stimulation.

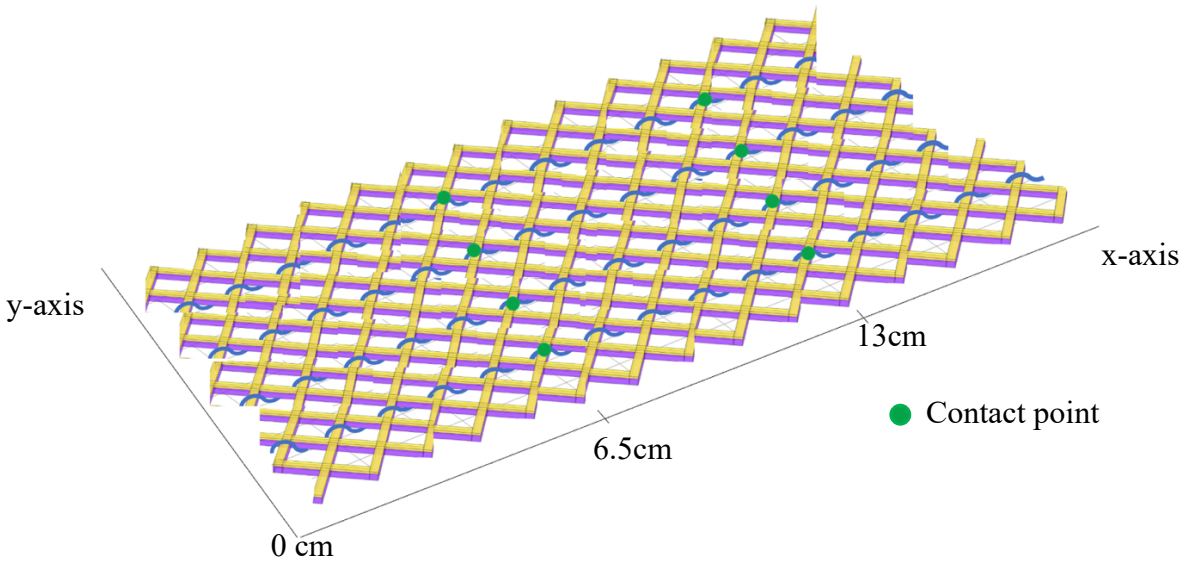

Figure 20. Large scale mesh design where unit models connected make up a larger product of a continuous mesh that can be cut to size and need. Possible spacing of contact points noted in green.

The future product application of the insulated conductive unit model requires that each insulated connection point be a small distance apart, relative to hernia size, to ensure the full region around the hernia receives at least a moderate level of EF. Anitha et al. (2018) found that the average size of mesh used in hernia repair is 7.5x7.5cm to 7.5x15cm [56]. A large-scale production of conductive mesh (the proposed future product with continual connections of the unit model) also needs a set distance at which the woven insulated wire makes contact with the conductive mesh surface. This contact point would be the location at which the anode/cathode creates the opposite side of the EF. An average spacing of the contact points is proposed to be every 6.5cm, based on the average hernia mesh used in surgery and to accommodate smaller than the stated average hernias. However, a future production of this product could instead consider a product line with small, medium, and larger spacing between contact points and insulated connections to facilitate the individual patient needs.

3.5.1 Limitations

One of the limitations found within any computational model is the gap between what is possible to model and what is known to be possible outside of the computation in a physical model. For example, COMSOL® multiphysics, while a very powerful and useful tool, cannot currently model any design with components smaller in size than 1/10000 of the largest component dimension in the model. This limitation is due to the mathematical relationship of the function f(x) = $\frac{1}{x}$. As the limit of x in the function f(x) goes to infinity, the function goes to zero ($\lim_{x\to\infty} \frac{1}{x} = 0$). To compute the FEA, COMSOL's hardware uses partial differential equations (PDE) to approximate the model to what would be the values in a physical model [57]. This is similar in concept to how integration takes slices of infinitesimally small thicknesses to solve for

the area under a function curve. While 10,000 is not very close to the value of infinity, any function with a denominator much larger or increasing faster than its numerator will force the function to approach 0. This is why the FEA solving becomes more difficult and time consuming for the computational aspect, since the elements within the FEA mesh are approaching an infinitely small area. COMSOL does not directly state why they chose to use the limitation of 1/10000. However, the computational power that is required to solve smaller and smaller elements may be outside of the program's capability at this time.

For this study, that smallest component limitation was a thickness of 548nm since one component had a depth (y length) of 5.48mm. From literature review and practical applications, it is not necessary or logical to use a conductive metal thickness of 20,000nm for this product design. But with this being acknowledged, it can be taken into account when considering the results from the unit model.

Another limitation within this study is the 3D constructed view of the hernia mesh. The actual woven monofilament diameters are 0.0125mm, which had to be approximated in the model to a group thickness of 0.2mm. Even though the pores between monofilaments are very small, they are assumed to not exist within the study model and cannot be accounted for in this computation of conductance or electric field. Furthermore, the woven joints at intersection of monofilaments are flexible and are designed to allow movement. By assuming the mesh is a rigid and has larger solid filaments of 0.2mm wide, the metal conductive layer cannot be verified in this computational model to allow movement at all, or that upon movement, the conductive layer would still be connected to conduct the current for the circuitry. Additionally, since the insulated model was compared to the unit model with the furthest separation of anode/cathode, two variables were changed: anode/cathode placement and the addition of the insulated wire. It was

determined that the lower EF in the insulated model was due to closer anode/cathode, but the effect of the insulated material on the EF through the PBS solution should be studied. Due to these limitations, the unit model is considered idealized.

The tissue targeted for cellular proliferation and overall strengthening in hernia repair is soft tissues. But there are many different cell types within that generic tissue location. This study picked fibroblasts since they are essential to the skin and muscle healing, and the literature reviews agreed that fibroblasts respond to electrical stimulation promptings for proliferation [3,4,18,19]. What is not considered is that the proliferation range of EF for fibroblasts used in this model may be determinantal to another cell type in the same region. Without researching all the impacts an electric field intensity has on the cells for a given soft tissue region, an *in vivo* study using this model would be assuming a lot of factors are negligible.

In regard to what AC and DC is on a fundamental level, there is some question as to what happens within the conductive materials as an EF is created. Since this study was designed to show a maximum EF range across a conductive hernia mesh, it is possible the difference in maximum EF between the DC and AC model comparisons is due to the AC capabilities that DC does not have. Furthermore, since the maximum EF values were measured from the peak amplitude timepoint within the AC frequency, this AC model does not actually represent time. This model shows a snapshot of an AC stimulation that could be for all intents and purposes a DC model and the 1MHz frequency would not matter. This comparison of AC/DC and the factors that control their function within COMSOL® is not directly known and therefore limits the conclusions that can be made at this time without further studies.

3.6 Conclusion

By comparing the electric fields for fibroblast cellular proliferation with the range of electric fields created by a voltage sweep in this COMSOL® computational model of electrically conductive hernia mesh, the voltages noted by Norman (2021) that can be produced from a piezoelectric device should be achievable to replicate in this modeled product design. A small piezoelectric device or other voltage source would be attached to the conductive metal coated polymer mesh to produce an electric field across the hernia mesh area to encourage fibroblasts nearby to proliferate and strengthen the weakened tissues. Based on the results of this unit model and recent research publications, this model used within the input voltage range of 20mV – 250 mV, would increase cellular proliferation of fibroblasts. The single unit electrically conductive hernia mesh COMSOL® model is not only a steppingstone towards reducing recurrence through cellular proliferation, but also a step towards better wound healing in all parts of the body where fibroblasts may be found.

3.7 Future Work

In continuation of this study, a verification of the electric field produced in this model through the surrounding PBS solution should be done. Direct measuring of EF in solution is difficult to do due to measuring probes in solution changing the EF as they enter the field [58]. A cellular proliferation *in vitro* study could be measured instead by quantifying the number of cells in a voltage sweep, and then comparing the confluence of the cells at the different voltage levels to other research studies for specified EF, circumventing the issues surrounding EF measuring. This would possibly indicate how close the COMSOL® model's values are to the actual EF the cells would experience *in vitro.*

Within the 3D model of this mesh design, it was found that as the EF propagates from the mesh surface outward in the YZ plane, the YZ maximum may not be the same as the maximums found in the XY plane. In order to predict the most accurate voltage input range for fibroblast proliferation, a voltage sweep across the mesh at intervals should be conducted and compared to the XY voltage sweep (Table 2).

For the material chosen to be the metal electrode layer, physical comparisons should be done that test adhesion and flaking during handling. A mesh called TiMESH, made by PFM Medical Inc., is a mesh available for surgical use [59]. Since this company already has a measure of success with this product, it would be prudent to test titanium as an electrode layer *in vitro* as well. Since titanium does have a capacity to conduct current, it could be a viable electrode metal choice.

The surface chemistry of the mesh and metal, while known to some degree due to general material properties, should be checked to ensure the mesh's hydrophobic nature is not compromised by any steps taken in coating and that the tissues in vivo would not adhere to the mesh. Hydrophobic/hydrophilic tests could be done simply measuring the contact angle of the material surface, but other surface characterizations such as SEM, Raman scattering, and infrared spectroscopy would be beneficial for noting other material properties not readily observed.

Another important question that needs to be determined before this model can be developed into a product is how the conductive mesh filaments will interact with each other *in vitro* if an AC stimulation causes secondary EF's and "eddies" (parallel resonance) in nearby conductive materials [52,60]. While the mesh conductive surface may be one unit, the individual mesh filaments may interfere with each other due to being parallel. COMSOL® is a multiphysics FEA modeling software and may be capable of predicting the parallel resonance, but the small

nature of this model makes it difficult to determine. Future studies will need to determine all this and other questions yet to be determined.

3.8 References

1. Wang See, C., Kim, T., & Zhu, D. (2020). Hernia mesh and hernia repair: A Review. *Engineered Regeneration*, *1*, 19–33. https://doi.org/10.1016/j.engreg.2020.05.002

2. Bredikhin, M., Gil, D., Rex, J., Cobb, W., Reukov, V., & Vertegel, A. (2020). Anti-inflammatory coating of hernia repair meshes: A 5-rabbit study. *Hernia*, *24*(6), 1191–1199. https://doi.org/10.1007/s10029-020-02122-9

3. Bhang, S. H., Jang, W. S., Han, J., Yoon, J.-K., La, W.-G., Lee, E., Kim, Y. S., Shin, J.-Y., Lee, T.-J., Baik, H. K., & Kim, B.-S. (2016). Zinc oxide nanorod-based piezoelectric dermal patch for wound healing. *Advanced Functional Materials*, *27*(1), 1603497. https://doi.org/10.1002/adfm.201603497

4. Chen, C., Bai, X., Ding, Y., & Lee, I.-S. (2019). Electrical stimulation as a novel tool for regulating cell behavior in tissue engineering. *Biomaterials Research*, *23*(1). https://doi.org/10.1186/s40824-019-0176-8

5. Thrivikraman, G., Boda, S. K., & Basu, B. (2018). Unraveling the mechanistic effects of electric field stimulation towards directing stem cell fate and function: A tissue engineering perspective. *Biomaterials*, *150*, 60–86. https://doi.org/10.1016/j.biomaterials.2017.10.003

6. Rouabhia: Rouabhia, M., Park, H., Meng, S., Derbali, H., & Zhang, Z. (2013). Electrical stimulation promotes wound healing by enhancing dermal fibroblast activity and promoting myofibroblast transdifferentiation. *PLoS ONE*, *8*(8). https://doi.org/10.1371/journal.pone.0071660

7. Alters, M. (2019). *Determination of Clinical Efficacy of Ultrasound Stimulation on Piezoelectric Composites for Power Generation Applications* (dissertation). ProQuest Dissertations Publishing, Lawrence, KS.

8. Center for Devices and Radiological Health, Hernia surgical mesh implants, U.S. Food and Drug Administration. (n.d.). https://www.fda.gov/medical-devices/implants-and-prosthetics/hernia- surgical-meshimplants (accessed October 13, 2021).

9. Kulacoglu, H. (2015). Current options in umbilical hernia repair in adult patients. *Turkish Journal of Surgery*. https://doi.org/10.5152/ucd.2015.2955

10. Arnaud, J. P., Hennekinne-Mucci, S., Pessaux, P., Tuech, J. J., & Aube, C. (2003). Ultrasound detection of visceral adhesion after intraperitoneal ventral hernia treatment: A comparative study of protected versus unprotected meshes. *Hernia*, *7*(2), 85–88. https://doi.org/10.1007/s10029-003-0116-2

11. Bueno-Lledó, J., Torregrosa-Gallud, A., Sala-Hernandez, A., Carbonell-Tatay, F., Pastor, P. G., Diana, S. B., & Hernández, J. I. (2017). Predictors of mesh infection and explantation after abdominal wall hernia repair. *The American Journal of Surgery*, *213*(1), 50–57. https://doi.org/10.1016/j.amjsurg.2016.03.007

12. Hori, T., & Yasukawa, D. (2021). Fascinating history of groin hernias: Comprehensive recognition of anatomy, classic considerations for Herniorrhaphy, and current controversies in Hernioplasty. *World Journal of Methodology*, *11*(4), 160–186. https://doi.org/10.5662/wjm.v11.i4.160

13. Burger, J. W. A., Luijendijk, R. W., Hop, W. C. J., Halm, J. A., Verdaasdonk, E. G. G., & Jeekel, J. (2004). Long-term follow-up of a randomized controlled trial of suture versus mesh repair of incisional hernia. *Annals of Surgery*, *240*(4), 578–585. https://doi.org/10.1097/01.sla.0000141193.08524.e7

14. Bhardwaj, N., Devi, D., & Mandal, B. B. (2014). Tissue-engineered cartilage: The crossroads of biomaterials, cells and stimulating factors. *Macromolecular Bioscience*, *15*(2), 153–182. https://doi.org/10.1002/mabi.201400335

15. Guo, A., Song, B., Reid, B., Gu, Y., Forrester, J. V., Jahoda, C. A. B., & Zhao, M. (2010). Effects of physiological electric fields on migration of human dermal fibroblasts. *Journal of Investigative Dermatology*, *130*(9), 2320–2327. https://doi.org/10.1038/jid.2010.96

16. Schäfer, M., & Werner, S. (2007). Transcriptional control of wound repair. *Annual Review of Cell and Developmental Biology*, *23*(1), 69–92. https://doi.org/10.1146/annurev.cellbio.23.090506.123609

17. Chang, Y., Li, H., & Guo, Z. (2014). Mesenchymal stem cell-like properties in fibroblasts. *Cellular Physiology and Biochemistry*, *34*(3), 703–714. https://doi.org/10.1159/000363035

18. Buckley, C. D. (2021). Fibroblast cells reveal their ancestry. *Nature*, *593*(7860), 511–512. https://doi.org/10.1038/d41586-021-01204-7

19. Mendias, C. L. (2017). Fibroblasts take the centre stage in human skeletal muscle regeneration. *The Journal of Physiology*, *595*(15), 5005–5005. https://doi.org/10.1113/jp274403

20. *Fibroblast*. Fibroblast | Cell Applications. (n.d.). Retrieved May 25, 2022, from https://www.cellapplications.com/fibroblast

21. Sadava, E. E., Krpata, D. M., Gao, Y., Rosen, M. J., & Novitsky, Y. W. (2013). Wound healing process and mediators: Implications for modulations for hernia repair and mesh integration. *Journal of Biomedical Materials Research Part A*, *102*(1), 295–302. https://doi.org/10.1002/jbm.a.34676

22. Kendall, R. T., & Feghali-Bostwick, C. A. (2014). Fibroblasts in fibrosis: Novel roles and mediators. *Frontiers in Pharmacology*, *5*. https://doi.org/10.3389/fphar.2014.00123

23. Norman, A. (2021). *Determination of a Clinically Relevant Tissue Phantom for Transcutaneous Ultrasound Stimulation of Piezoelectric Discs for Current Density Applications* (thesis). University of Kansas, Lawrence.

24. Speed: C.A. Speed, Therapeutic ultrasound in soft tissue lesions, Rheumatology. 40 (2001) 1331–1336. doi:10.1093/rheumatology/40.12.1331.

25. Berbel, G. (2021). *Hernia - 101*. *Hernia Repair Research Project*. Lawrence; University of Kansas.

26. Sanbhal, N., Miao, L., Xu, R., Khatri, A., & Wang, L. (2017). Physical structure and mechanical properties of knitted hernia mesh materials: A Review. *Journal of Industrial Textiles*, *48*(1), 333–360. https://doi.org/10.1177/1528083717690613

27. Baylón, K., Rodríguez-Camarillo, P., Elías-Zúñiga, A., Díaz-Elizondo, J., Gilkerson, R., & Lozano, K. (2017). Past, present and future of surgical meshes: A Review. *Membranes*, *7*(3), 47. https://doi.org/10.3390/membranes7030047

28. Cobb, W. S., Peindl, R. M., Zerey, M., Carbonell, A. M., & Heniford, B. T. (2008). Mesh terminology 101. *Hernia*, *13*(1), 1–6. https://doi.org/10.1007/s10029-008-0428-3

29. Idrees, S., Jindal, S., Gupta, M., & Sarangi, R. (2018). Surgical meshes – the search continues. *Current Medicine Research and Practice*, *8*(5), 177–182. https://doi.org/10.1016/j.cmrp.2018.08.005

30. Developers, G. S. (n.d.). *Gauss's law for Electric Fields*. Gauss's Law for Electric Fields - Electromagnetic Geophysics. Retrieved June 7, 2022, from http://em.geosci.xyz/content/maxwell1_fundamentals/formative_laws/gauss_electric.html?highlight=gauss+law

31. *Multiphysics Cyclopedia*. COMSOL. (n.d.). Retrieved June 7, 2022, from https://www.comsol.com/multiphysics/electrostatics-theory

32. COMSOL. (n.d.). *Electrostatics Equations*. Electrostatics equations. Retrieved June 7, 2022, from https://doc.comsol.com/5.5/doc/com.comsol.help.acdc/acdc_ug_electric_fields.07.102.html

33. Tutor help desk. (n.d.). *Gauss law in Dielectrics*. tutorhelpdesk.com. Retrieved June 7, 2022, from https://www.tutorhelpdesk.com/homeworkhelp/Electricity-Magnetism-/Gauss-Law-In-Dielectrics-Assignment-Help.html

34. Bpf, British Plastics Federation, Polypropylene (PP). (n.d.).

https://www.bpf.co.uk/plastipedia/polymers/pp.aspx (accessed March 1, 2022).

35. Luis, E., Pan, H. M., Sing, S. L., Bastola, A. K., Goh, G. D., Goh, G. L., Tan, H. K., Bajpai, R., Song, J., & Yeong, W. Y. (2019). Silicone 3D printing: Process optimization, product biocompatibility, and reliability of silicone meniscus implants. *3D Printing and Additive Manufacturing*, *6*(6), 319–332. https://doi.org/10.1089/3dp.2018.0226

36. Han, T., Du, B., Ma, T., Wang, F., Gao, Y., Lei, Z., & Li, C. (2019). Electrical tree in HTV silicone rubber with temperature gradient under repetitive pulse voltage. *IEEE Access*, *7*, 41250–41260. https://doi.org/10.1109/access.2019.2907302

37. Zhang, X., Yi, J., Yin, Y., Song, Y., & Xiong, C. (2021). Thermal conductivity and electrical insulation properties of H-BN@PDA/silicone rubber composites. *Diamond and Related Materials*, *117*, 108485. https://doi.org/10.1016/j.diamond.2021.108485

38. Koh, K. M. (2016). *Effects of alternating current electrical stimulation on the cellular chemistry and proliferation of C2C12 muscle cells* (thesis). ProQuest LLC, Ann Arbor.

39. Tao, C. (2018). Antimicrobial activity and toxicity of gold nanoparticles: Research progress, challenges and prospects. *Letters in Applied Microbiology*, *67*(6), 537–543. https://doi.org/10.1111/lam.13082

40. Selvaraj, V., Grace, A. N., Alagar, M., & Hamerton, I. (2010). Antimicrobial and anticancer efficacy of antineoplastic agent capped gold nanoparticles. *Journal of Biomedical Nanotechnology*, *6*(2), 129–137. https://doi.org/10.1166/jbn.2010.1115

41. Heymann, F., von Trotha, K.-T., Preisinger, C., Lynen-Jansen, P., Roeth, A. A., Geiger, M., Geisler, L. J., Frank, A. K., Conze, J., Luedde, T., Trautwein, C., Binnebösel, M., Neumann, U. P., & Tacke, F. (2019). Polypropylene mesh implantation for hernia repair causes myeloid cell–driven persistent inflammation. *JCI Insight*, *4*(2). https://doi.org/10.1172/jci.insight.123862

42. *Phosphate buffered saline solution, 10x concentrate*. AmericanBio. (n.d.). Retrieved May 26, 2022, from https://www.americanbio.com/product/AB11072

43. Binachi, E., Bellati, F. M., Rollo, E., Dubini, G., & Guiducci, C. (2021). Model Of An Interdigitated Electrodes System For Cell Counting Based On Impedance Spectroscopy. *Excerpt from the Proceedings of the 2021 COMSOL Conference in Milan*. https://doi.org/https://www.comsol.ru/paper/download/152565/bianchi_abstract.pdf

44. Salmanzadeh, A., Sano, M. B., Gallo-Villanueva, R. C., Roberts, P. C., Schmelz, E. M., & Davalos, R. V. (2013). Investigating dielectric properties of different stages of syngeneic murine ovarian cancer cells. *Biomicrofluidics*, *7*(1), 011809. https://doi.org/10.1063/1.4788921

45. From Thermo Fisher Scientific – Solutions for Industrial and Safety Applications, From PerkinElmer Food Safety and Quality, Analytics, F. K. P. M., Inovenso, F., Control, F. T. M. C. V., Corp., F. M.-S., & From Thermo Fisher Scientific – Electron Microscopy Solutions. (2017, November 20). *Properties: Silicone rubber*. AZoM.com. Retrieved May 26, 2022, from https://www.azom.com/properties.aspx?ArticleID=920

46. *Electrical Conduction in Semiconductors*. MKS. (n.d.). Retrieved May 26, 2022, from https://www.mksinst.com/n/electrical-conduction-semiconductors

47. *Volume resistivity*. Volume Resistivity: Electrical Resistivity of Plastic. (n.d.). Retrieved May 26, 2022, from https://omnexus.specialchem.com/polymer-properties/properties/volume-resistivity

48. *Dielectric constant*. Dielectric Constant: Definition, Units, Formula, Plastic Values &Material List. (n.d.). Retrieved May 26, 2022, from https://omnexus.specialchem.com/polymer-properties/properties/dielectric-constant

49. COMSOL Multiphysics® v. 6.0. www.comsol.com. COMSOL AB, Stockholm, Sweden.

50. *Material: Gold (PVD or electroplated)*. 6.777J/2.751J Material Property Database. (n.d.). Retrieved May 26, 2022, from https://www.mit.edu/~6.777/matprops/gold.htm

51. *Dielectric constants of various materials*. Clipper Controls. (n.d.). Retrieved May 26, 2022, from https://www.clippercontrols.com/pages/Dielectric-Constant-Values.html#P

52. Weststrate, E., Steinback, M., Rensing, N. M., & Tiernan, T. (2010). COMSOL Multiphysics Modeling for Design Optimization of Eddy Current Crack Detectors. *Excerpt from the Proceedings of the COMSOL Conference 2010 Boston*. https://doi.org/https://www.comsol.com/paper/comsol-multiphysics-modeling-for-design-optimization-of-eddy-current-crack-detec-9083

53. Efis: Clean Line Energy Partners. (2011). *Understanding Electric and Magnetic Fields*. Public Service Commission. Retrieved May 31, 2022, from https://www.efis.psc.mo.gov/mpsc/commoncomponents/viewdocument.asp?DocId=

54. COMSOL Multiphysics. (n.d.). *Frequency Domain Study*. Frequency domain study. Retrieved May 31, 2022, from https://doc.comsol.com/5.5/doc/com.comsol.help.aco/aco_ug_study_types.15.04.html

55. The Royal Academy of Engineering. (n.d.). *The study of Root Mean Square (RMS) value*. Retrieved June 1, 2022, from https://www.raeng.org.uk/publications/other/8-rms

56. Anitha, B., Aravindhan, K., Sureshkumar, S., Ali, M. S., Vijayakumar, C., & Palanivel, C. (2018). The ideal size of mesh for open inguinal hernia repair: A morphometric study in patients with inguinal hernia. *Cureus*. https://doi.org/10.7759/cureus.2573935827678

57. *Multiphysics Cyclopedia*. COMSOL. (n.d.). Retrieved June 7, 2022, from https://www.comsol.com/multiphysics/finite-element-method

58. Doi, K., Asano, N., & Kawano, S. (2020). Development of glass micro-electrodes for local electric field, electrical conductivity, and ph measurements. *Scientific Reports*, *10*(1). https://doi.org/10.1038/s41598-020-60713-z

59. Timesh Hernia Mesh, PFM Medical, Inc. (2020). https://www.pfmmedicalusa.com/timesh/ (accessed January 22, 2022).

60. *Parallel resonance and parallel RLC Resonant Circuit*. Basic Electronics Tutorials. (2018, October 15). Retrieved May 31, 2022, from https://www.electronics-tutorials.ws/accircuits/parallel-resonance.html

Appendix A: Preliminary Testing for Electrode Metal Coating

Abstract

Hernia repair with the incorporation of a support mesh significantly reduced the numbers of recurrence seen in patients to 32% [1,2)]. This percentage of individuals is still very large and should be reduced by modifying the methods or materials used in hernioplasty. In general, recurrence is due to the weakened tissues at the site of the hernia still being weak and under the same, if not more, strain, which results in the hernia retearing. Since electrical stimulation of tissues has shown to encourage cellular proliferation, it is reasonable to expect similar results by the incorporation of an electric field across the hernia mesh [3]. The proposed method of achieving this utilizes a thin conductive layer of gold added to the surface of polypropylene hernia mesh. Several methods of gold application to the mesh were examined and tested, but the only method that could be done and showed success was by sputter coating. Not only did the gold layer adhere well to the surface when handled and mechanically stretched, but the conductivity across the mesh also showed positive results since the sputter coating allowed for all points across the woven mesh to be connected. The method of sputter coating gold onto the surface of polypropylene hernia mesh proved to be the best for continued research in this study.

Introduction

Mesh Properties

Hernioplasty is the surgical procedure and use of support mesh for addressing hernia wounds. Hernioplasty was developed as a continuation of herniorrhaphy, which only sutured the hernia wound and did not use mesh [4]. Since then, hernioplasty became the accepted practice for hernia repair and because of this, the development of new and optimized mesh began. Polypropylene (PP) was one of the first materials that showed good results in tissue acceptance

and reduced recurrence [5]. Part of PP's success in hernia repair is due to its hydrophobicity that prevents the tissues from adhering [6,7]. The other major contributor to PP's positive results is its mechanical characteristics and their approximation to the native tissue's density and toughness [2]. Matching the tissues mechanical strengths is crucial to ensure the mesh supports the weakened area. If the mesh is too elastic, the hernia site may retear [2,8,9]. Mesh that is too rigid causes the sutured anchor points of the mesh to pull on the tissues when the tissues stretch, that not only causes pain for the individual but also can cause other hernias in the region [10]. Because of these issues, an effective hernioplasty should use a mesh that matches the tissues' mechanical characteristics as closely as possible.

Despite the positive attributes of PP and other meshes used in hernioplasty, the numbers of recurrence, the retearing of a previous hernia site, have only dropped from 63% to 32% [1,2, 11]. Recurrence should not be a prevalent event, given that over a million individuals have hernia repair surgery every year [12,13]. With an effective hernia repair using mesh, there should be far fewer recurrence incidents.

To achieve the desired results of fewer recurrence, the current mesh being used requires something more or an adaptation. With the use an electrical stimulation, the tissues could be prompted to not only heal more quickly, reducing the time an infection could occur, but the greater number of cells in the region would strengthen the region near the stimulation [3,14]. Positive results show electrically stimulated cells can be influenced to move perpendicular to a wound when an electric field is placed across the wound, which is called electrotaxis [15]. Since the body physiology relies heavily on electric potentials, wounds in the soft tissue already show an endogenous electric field (EF) of 100-200 mV/mm [16]. Any additional electrical stimulation then enhances the speed in which the healing process occurs [16-18]. This incorporation of an

electrical field across a hernia mesh requires the addition of a conductive material by which the current can be carried.

Electrode Materials

In choosing the material best suited for conducting a small current inside the body, the material's biocompatibility is of upmost importance. The second characteristic for the electrode material is conductivity. Several materials that are biocompatible and conductive would be effective but can become toxic to the body when nanometer size particles migrate into the tissues [19]. The materials that meet these three general requirements (biocompatible, conductive, and non-toxic) are gold, platinum, and titanium. Each of these materials are used in current medical devices, but gold and platinum are significantly more conductive (Table 4). When the materials were compared in COMSOL®, a metaphysis finite element analysis software, a model of the electric fields showed some differences in electric field intensity, but that is negligible when the voltage input can be adjusted to meet the intensity desired for cellular stimulation. Material cost should also be considered in a medical device, and although all the materials are received well by the native tissues, gold and platinum are considerably more expensive to use in a device than the same amount of titanium [20-22]. Overall, gold and platinum are more conductive than titanium, but both gold and platinum are expensive, the choice in material is then determined by ease of use and attainability. For the three options considered for adding a conductive layer, gold was the most versatile and attainable in forms for multiple application methods.

Table 5: Possible electrode materials and their attributes			
Material	**Biocompatibility**	**Conductance (S)**	**Cost 2”x0.125’**
Gold[20]	Excellent	4.37e7	$10,598.00
Platinum[21]	Ideal	9.43e6	$7,150.00
Titanium[22]	Highest Rated	7.407e5	$90.00

Methods

Mesh Preparation

Each gold application method was tested on a 10x10cm of polypropylene mesh (PPKM505 58 GSM) from Surgical Mesh™ Division Textile Development Associates, Inc.. The mesh samples were cut from a larger roll and the edges left raw, and the gold samples used for coating were rated at 99% purity or greater.

Electrode Coating

Hot Melt

The first method tried utilized a hot iron to melt a thin gold foil layer to the surface. Since the melting temperature of gold (1064°C) is significantly higher than polypropylene’s melting point (160°C), the temperature of the iron was set to under the PP melting point. Since the PP fibers were so thin, only the surface of the mesh required warming to adhere the mesh to the foil.

Liquid Application

The second method for adding a layer of gold to the mesh was unable to be performed due to lack of biologically safe liquid forms of gold. If attained, the mesh could be coated by thin and evening brushing of the paint or laying the mesh sample into a thin poured layer of the paint.

Aerosolized gold paint was also considered, but without the right airbrushing equipment, it was still not able to be tested.

Adhesive

Similar to the hot melt method, the method of adhering a gold layer utilized a thin foil. A few medical grade adhesives were looked into, but most of them stipulated they were only for external use. Common glue could have used for proof of concept, but without a readily attainable biologically safe adhesive for internal use, this method was not deemed the best method to move forward with.

Sputter coating

Sputter coating, the last application option considered, used an EMS150R S Quorum with a rotating stage for even coating (Figure 21). The mesh samples were placed on glass slides and fixed in place with double sided lab grade tape to prevent the mesh from falling off during the process. Since gold is one of the common sputter targets used, the machine had pre-set programs that could be selected. The program parameters for a gold target and 100nm of deposition were current (60 mA), chamber pressure ($1x10^{-1}$ Pa), with a deposition rate of 13-20 nm/min at a density of 19.32 g/m^3. After the sputter cycle was complete and the chamber depressurized, the samples were removed from the glass slide and pressed flat to prevent curvature and for later ease of handling.

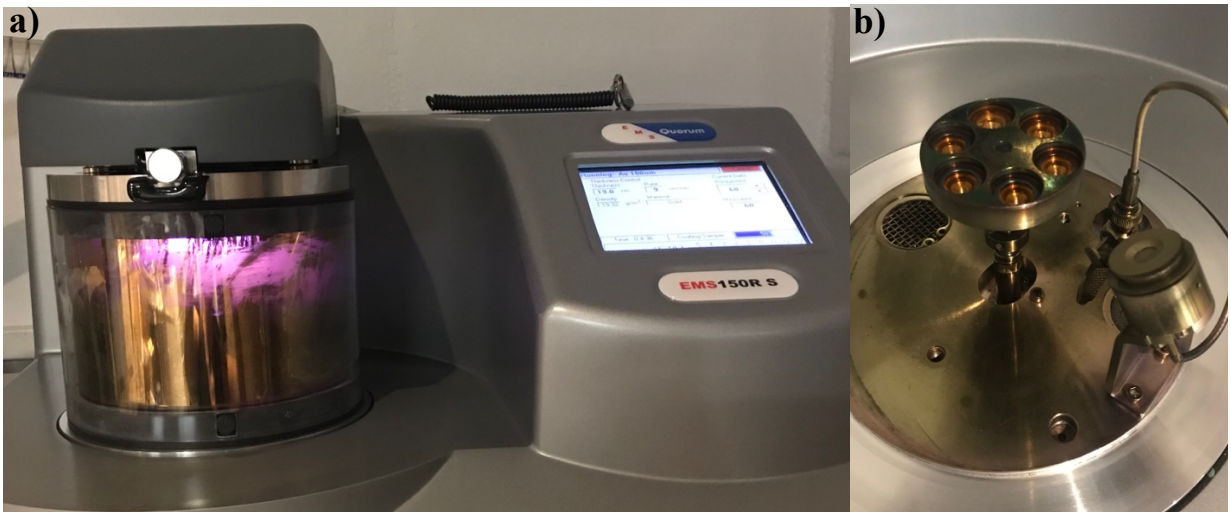

Figure 21. a) EMS150R S Quorum sputter coater used to create electrode gold layer, and **b)** rotational stage inside the sputter chamber.

Adhesion and Conductivity Tests

After the gold was adhered to the mesh, the samples from the two application methods were tested for strength of adhesion and conductivity. According to ASTM B571 that stipulates adhesion testing methods for electrodeposition of gold, the samples were bent repeatedly, scraped lightly and handled, stretched repeatedly in all directions, and peeled using adhesive tape [25]. Conductivity was tested by a use of voltmeter (AMPROBE 34XR-A**)** that measured the resistance between two points on the surface at increasing distances.

Results

Hot Melt

The use of a hot iron to melt only the very surface of the mesh for adhering to the gold foil was, in short, not effective. Not only was the iron difficult to adjust to the right temperature to prevent melting, but the nature of the gold foil made it often appear to be adhering to the mesh through static electricity. When the iron was too hot, the mesh melted to the point of complete

melting and deformation. An iron at too low of a temperature allowed the gold to flake off when it was touched or brushed (Figure 22**).** Both resulted in a gold coating that would not allow conduction of a current across it since continuity of the gold was sporadic.

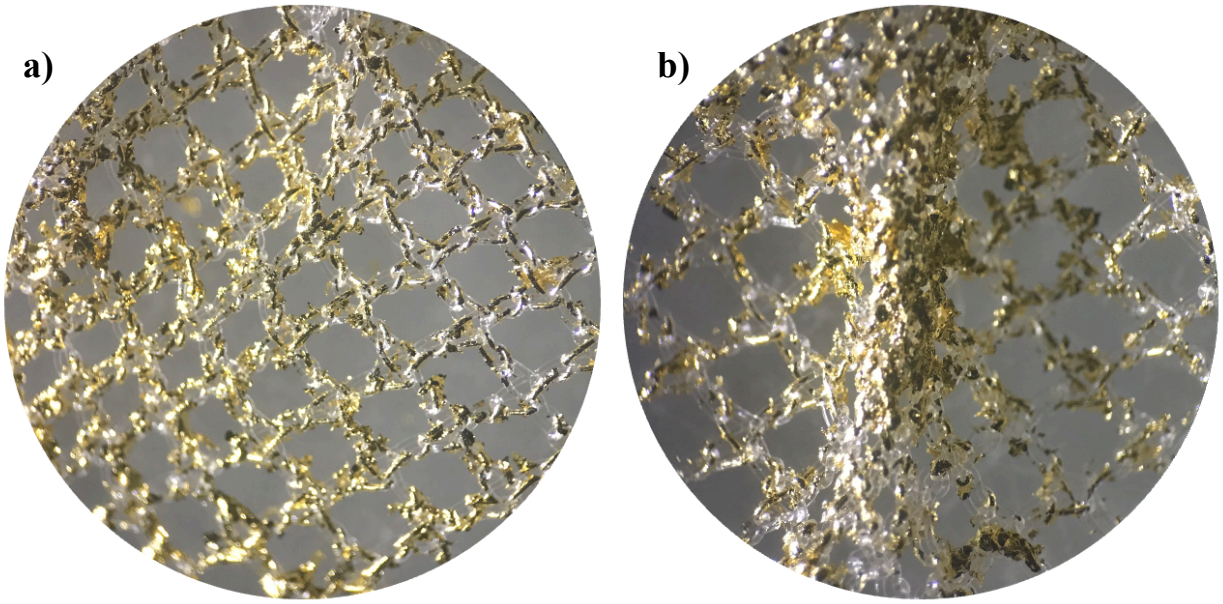

Figure 22. Hot melt gold foil application where **a)** gold held by static electricity until disturbed and easily brushed off and **b)** shows a shriveled section that melted under too high of heat.

Sputter Adhesion

For most samples that were sputter coated, the visual results showed an even and continuous gold layer over the mesh surface. The gold adhesion tests also showed very minimal gold flaking from handling, light scraping, mechanical stretching, and removal by another adhesive surface and conductivity was still reading from opposite sides of mesh (Figure 23**).** There was some issue with the sputter coating process, in the event the mesh was not well adhered to the glass slide, where the mesh would become heated and curl into itself as the PP melted in outer regions that were too near the target.

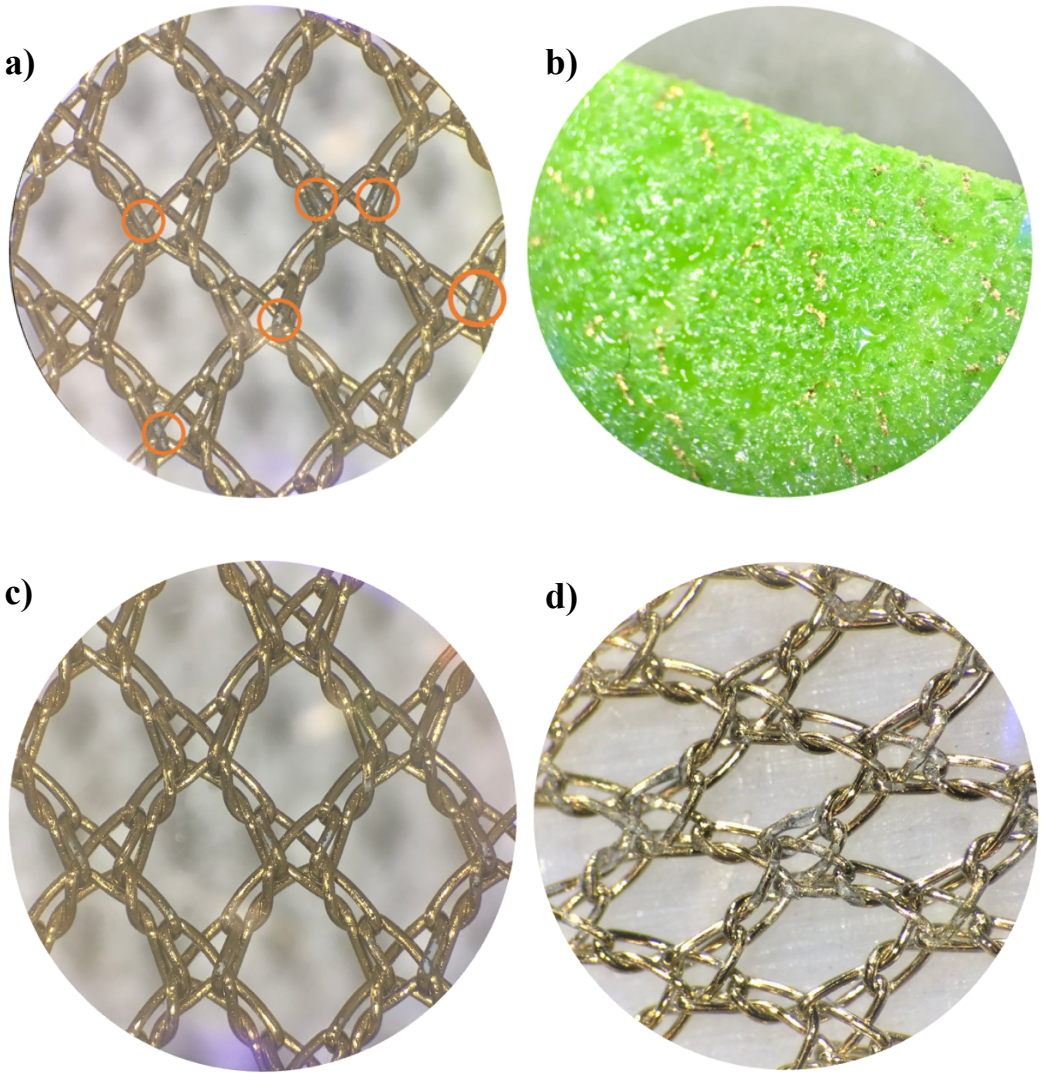

Figure 23. Adhesion tests that show **a)** locations of gold missing where **b)** adhesive tape lifted small parts of gold away. **c)** Minimal flaking or gold loss from mechanical stretching and **d)** gold left after light scraping.

Electrical Capability

Since the gold foil melt did not show connected and continuous gold, there was no reason to test its conductive capacity and resistance. The sputter coated samples, however, showed continuous gold connection and therefore conduction at all points and distances. Resistance

readings were small, and therefore often difficult to read from the voltmeter, but the sputter coated mesh was conductive even after the mesh sample had been handled and stretched repeatedly.

Discussion

Due to the difficulty in handling of gold foil and the mesh being mechanically compromised, the hot melt of gold onto PP surface does not make it a viable option for continued use. The sputter coating, however, shows decent results for continued tested and moving towards *in vitro* studies. For the gold being used, it is important that it is medical grade and has a purity level greater than 99%. Since the goal for this electrically stimulated mesh is to use in *in vivo*, the allowable toxins should be almost none and non-toxic to the tissues. The thickness of the gold layer is also questionable, since other studies use anywhere from 5-500nm thickness of metal for cellular stimulation through electric fields [23,24]. For the purposes of this study and at a thickness of 100nm, the metal electrode showed good connectivity and little flaking, which was the general goal. This thickness should be verified for optimal product concept in later studies. Medical devices, when coated with gold through electrodeposition, do have standards for thickness, which may apply to this future device. The MIL-G-45204 (military grade) code for medical devices stipulates a minimum thickness of .00002 inch (508nm), which is significantly more than the thickness tested in this study but may not be applicable for this device design or be optimal for biocompatibility [25].

Conclusion

Considering the biocompatible and conductive materials used in medical devices, gold was the optimal material for preliminary testing for a hernia mesh electrode. The various methods tested for applying the gold to the mesh surface showed that sputter coating was

effective, efficient, and allowed for good conduction across the mesh, while melting a gold foil to the mesh was ineffective and mechanically compromised the polymer. For a conductive metal to be added to existing medical grade hernia mesh, the sputter coating of gold is the best method considered and tested in this study.

Future Work

As with any medical device intended for internal use, surface chemistry is an important factor. Polypropylene mesh is naturally hydrophobic, which prevents tissue bonding and chronic pain for patients [6,7]. A metal layer added would change this surface condition to the new material's characteristics. Thickness of the conductive metal should also be further tested *in vitro* to ensure the tissues are not harmed and the overall device design is optimized.

References

1. Burger, J. W. A., Luijendijk, R. W., Hop, W. C. J., Halm, J. A., Verdaasdonk, E. G. G., & Jeekel, J. (2004). Long-term follow-up of a randomized controlled trial of suture versus mesh repair of incisional hernia. *Annals of Surgery*, *240*(4), 578–585. https://doi.org/10.1097/01.sla.0000141193.08524.e7

2. Wang See, C., Kim, T., & Zhu, D. (2020). Hernia mesh and hernia repair: A Review. *Engineered Regeneration*, *1*, 19–33. https://doi.org/10.1016/j.engreg.2020.05.002

3. Kotnik, T., & Miklavčič, D. (2006). Theoretical evaluation of voltage inducement on internal membranes of biological cells exposed to electric fields. *Biophysical Journal*, *90*(2), 480–491. https://doi.org/10.1529/biophysj.105.070771

4. Hori, T., & Yasukawa, D. (2021). Fascinating history of groin hernias: Comprehensive recognition of anatomy, classic considerations for Herniorrhaphy, and current controversies in Hernioplasty. *World Journal of Methodology*, *11*(4), 160–186. https://doi.org/10.5662/wjm.v11.i4.160

5. Baylón, K., Rodríguez-Camarillo, P., Elías-Zúñiga, A., Díaz-Elizondo, J., Gilkerson, R., & Lozano, K. (2017). Past, present and future of surgical meshes: A Review. *Membranes*, *7*(3), 47. https://doi.org/10.3390/membranes7030047

6. Shokrollahi, M., Bahrami, S. H., Nazarpak, M. H., & Solouk, A. (2020). Biomimetic double-sided polypropylene mesh modified by DOPA and ofloxacin loaded carboxyethyl chitosan/polyvinyl alcohol-polycaprolactone nanofibers for potential hernia repair applications. *International Journal of Biological Macromolecules*, *165*, 902–917. https://doi.org/10.1016/j.ijbiomac.2020.09.229

7. Auriemma, F., Ruiz de Ballesteros, O., De Rosa, C., & Invigorito, C. (2011). Tailoring the mechanical properties of isotactic polypropylene by blending samples with different stereoregularity. *Macromolecules*, *44*(15), 6026–6038. https://doi.org/10.1021/ma201420f

8. Sanbhal, N., Miao, L., Xu, R., Khatri, A., & Wang, L. (2017). Physical structure and mechanical properties of knitted hernia mesh materials: A Review. *Journal of Industrial Textiles*, *48*(1), 333–360. https://doi.org/10.1177/1528083717690613

9. Heymann, F., von Trotha, K.-T., Preisinger, C., Lynen-Jansen, P., Roeth, A. A., Geiger, M., Geisler, L. J., Frank, A. K., Conze, J., Luedde, T., Trautwein, C., Binnebösel, M., Neumann, U. P., & Tacke, F. (2019). Polypropylene mesh implantation for hernia repair causes myeloid cell–driven persistent inflammation. *JCI Insight*, *4*(2). https://doi.org/10.1172/jci.insight.123862

10. De Keulenaer, B. L., De Waele, J. J., Powell, B., & Malbrain, M. L. (2009). What is normal intra-abdominal pressure and how is it affected by positioning, body mass and positive end-expiratory pressure? *Intensive Care Medicine*, *35*(6), 969–976. https://doi.org/10.1007/s00134-009-1445-0

11. Costello, C. R., Bachman, S. L., Ramshaw, B. J., & Grant, S. A. (2007). Materials characterization of explanted polypropylene hernia meshes. *Journal of Biomedical Materials Research Part B: Applied Biomaterials*, *83B*(1), 44–49. https://doi.org/10.1002/jbm.b.30764

12. Center for Devices and Radiological Health, Hernia surgical mesh implants, U.S. Food and Drug Administration. (n.d.). https://www.fda.gov/medical-devices/implants-and-prosthetics/hernia- surgical-meshimplants (accessed October 13, 2021).

13. Kulacoglu, H. (2015). Current options in umbilical hernia repair in adult patients. *Turkish Journal of Surgery*. https://doi.org/10.5152/ucd.2015.2955

14. Bhang, S. H., Jang, W. S., Han, J., Yoon, J.-K., La, W.-G., Lee, E., Kim, Y. S., Shin, J.-Y., Lee, T.-J., Baik, H. K., & Kim, B.-S. (2016). Zinc oxide nanorod-based piezoelectric dermal patch for wound healing. *Advanced Functional Materials*, *27*(1), 1603497. https://doi.org/10.1002/adfm.201603497

15. Thomas, A. D., & Rogers, A. (2004). Edoardo Bassini and the wound that inspires. *World Journal of Surgery*, *28*(10), 1060–1062. https://doi.org/10.1007/s00268-004-7466-5

16. Thrivikraman, G., Boda, S. K., & Basu, B. (2018). Unraveling the mechanistic effects of electric field stimulation towards directing stem cell fate and function: A tissue engineering perspective. *Biomaterials*, *150*, 60–86. https://doi.org/10.1016/j.biomaterials.2017.10.003

17. Chen, C., Bai, X., Ding, Y., & Lee, I.-S. (2019). Electrical stimulation as a novel tool for regulating cell behavior in tissue engineering. *Biomaterials Research*, *23*(1). https://doi.org/10.1186/s40824-019-0176-8

18. Guo, A., Song, B., Reid, B., Gu, Y., Forrester, J. V., Jahoda, C. A. B., & Zhao, M. (2010). Effects of physiological electric fields on migration of human dermal fibroblasts. *Journal of Investigative Dermatology*, *130*(9), 2320–2327. https://doi.org/10.1038/jid.2010.96

19. Sen, G. T., Ozkemahli, G., Shahbazi, R., Erkekoglu, P., Ulubayram, K., & Kocer-Gumusel, B. (2020). The effects of polymer coating of gold nanoparticles on oxidative stress and DNA damage. *International Journal of Toxicology*, *39*(4), 328–340. https://doi.org/10.1177/1091581820927646

20. *Kurt J. Lesker company*. Kurt J. Lesker Company. (n.d.). Retrieved May 6, 2022, from https://www.lesker.com/newweb/deposition_materials/depositionmaterials_sputtertargets_1.cfm?pgid=au1

21. *Kurt J. Lesker company*. Kurt J. Lesker Company. (n.d.). Retrieved May 6, 2022, from https://www.lesker.com/newweb/deposition_materials/depositionmaterials_sputtertargets_1.cfm?pgid=pt1

22. *Kurt J. Lesker company*. Kurt J. Lesker Company. (n.d.). Retrieved May 15, 2022, from https://www.lesker.com/newweb/deposition_materials/depositionmaterials_sputtertargets_1.cfm?pgid=ti1

23. Blume, G., Müller-Wichards, W., Goepfert, C., Pörtner, R., & Müller, J. (2013). Electrical stimulation of NIH-3T3 cells with platinum-PEDOT-electrodes integrated in a bioreactor. *The Open Biomedical Engineering Journal*, *7*(1), 125–132. https://doi.org/10.2174/1874120701307010125

24. Dowling, D. P., Donnelly, K., McConnell, M. L., Eloy, R., & Arnaud, M. N. (2001). Deposition of anti-bacterial silver coatings on polymeric substrates. *Thin Solid Films*, *398-399*, 602–606. https://doi.org/10.1016/s0040-6090(01)01326-8

25. *Requirements for medical grade gold plating*. Sharretts Plating Company. (2019, February 21). Retrieved May 4, 2022, from https://www.sharrettsplating.com/blog/requirements-medical-grade/

Appendix B: COMSOL® Workflow and Parameters Used

Selections to Begin New Model

Step 1: Select New "Model Wizard"
Step 2: Select Space Dimension, "3D"
Step 3: Select Physics, AC/DC, "Electric Currents (ec)" and "Electrostatics (es)"
Step 4: Select Study, "Time Dependent"

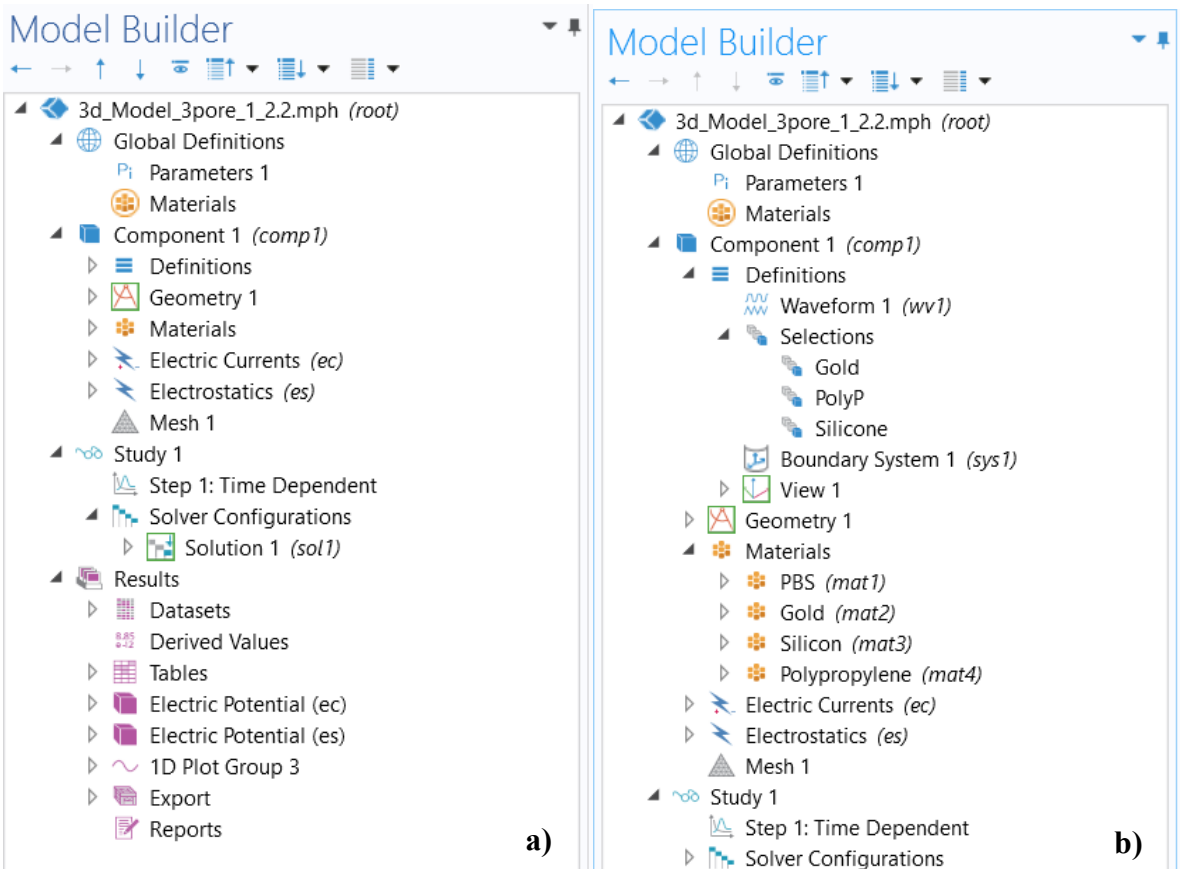

Figure 24. a) General workflow and parameter outline that shows result plots and **b)** with definitions and materials shown.

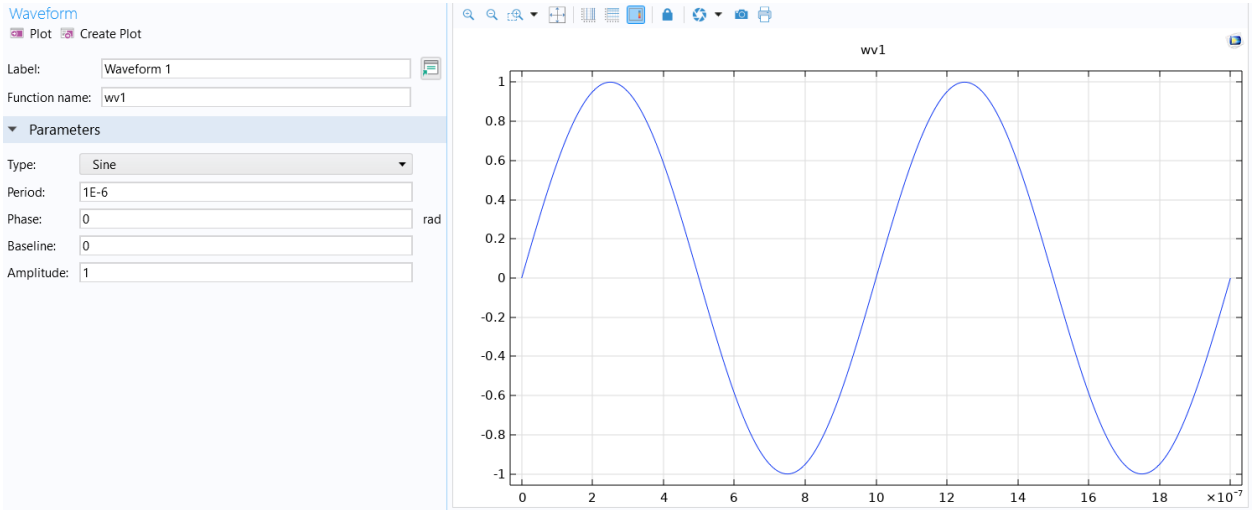

Figure 25. Waveform (wv1) of input voltage with a period of 1MHz and amplitude (V_{in}).

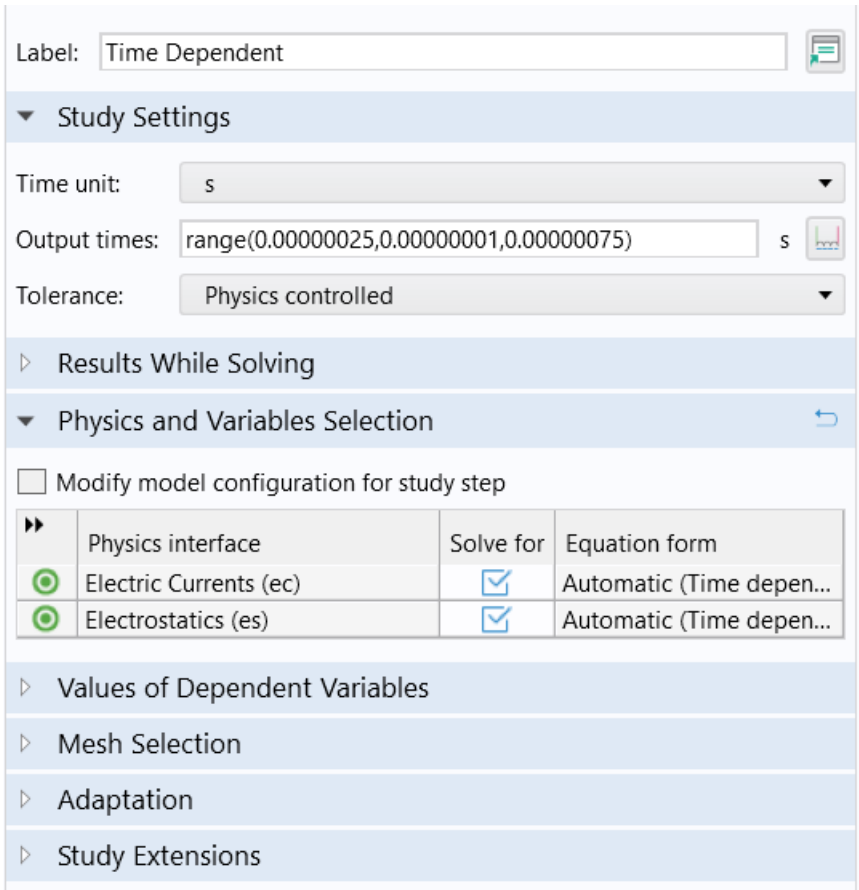

Figure 26. Study: Time Dependent based on frequency, from $2.5x10^{-7}$ to $7.5x10^{-7}$ (+peak to -peak) with a step size of 1x $x10^{-8}$.

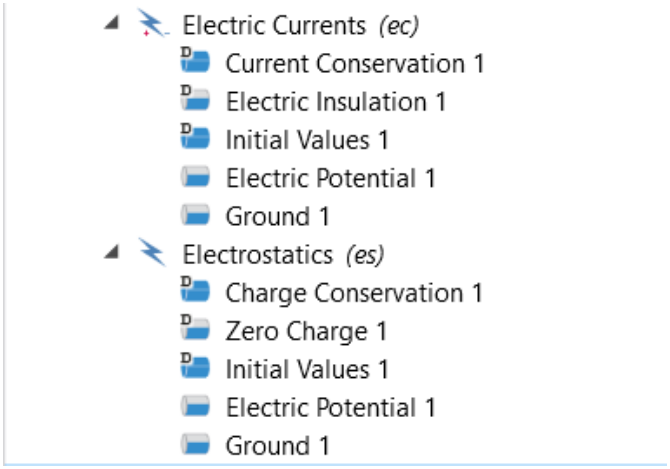

Figure 27. Auto populated ec and es model assignments for identifying circuit structure.

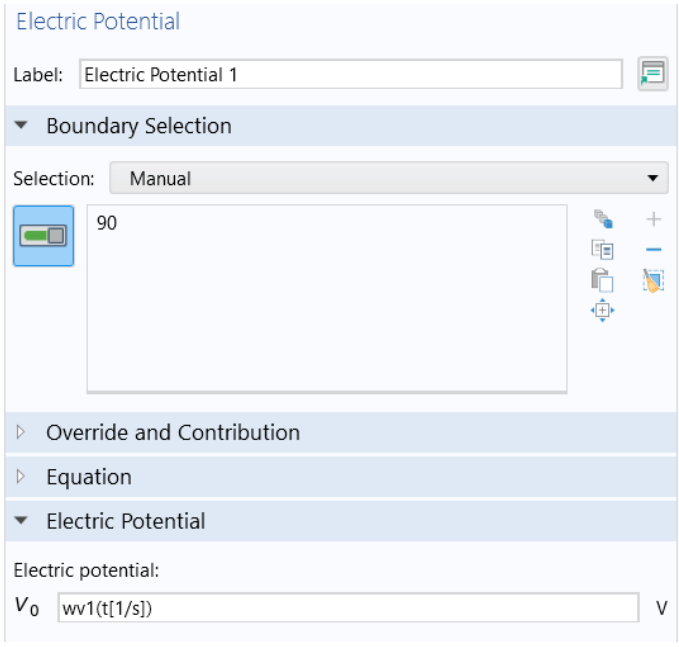

Figure 28. Electric potential assignment to element #90, with V_0 (voltage) dependent on wv1 as a function of t and inverse s.

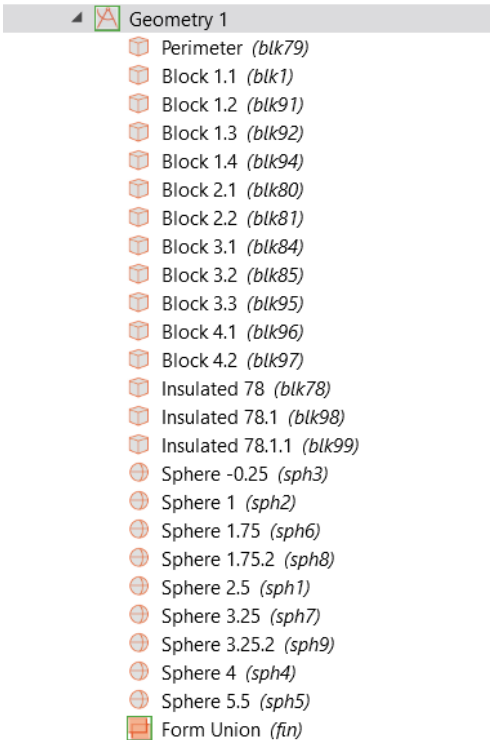

Figure 29. Geometry units for full model design.

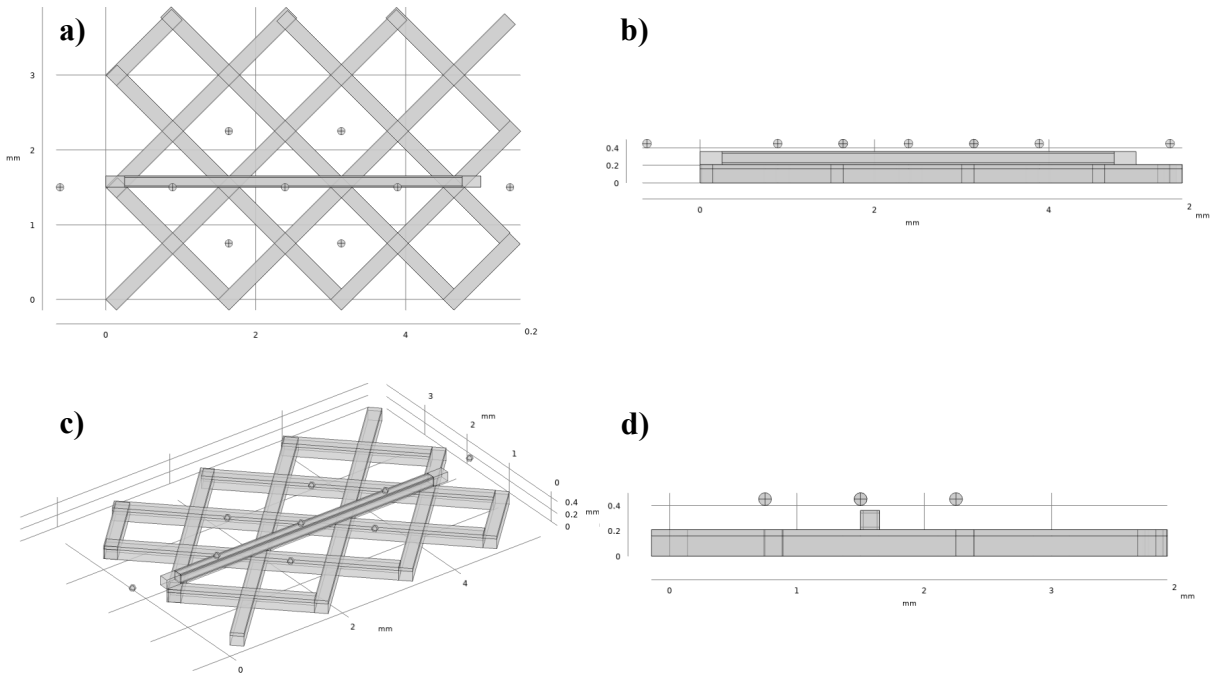

Figure 30. Geometry configuration in **a)** xy-axis, **b)** xz-axis, **c)** orthogonal and **d)** yz-axis views.

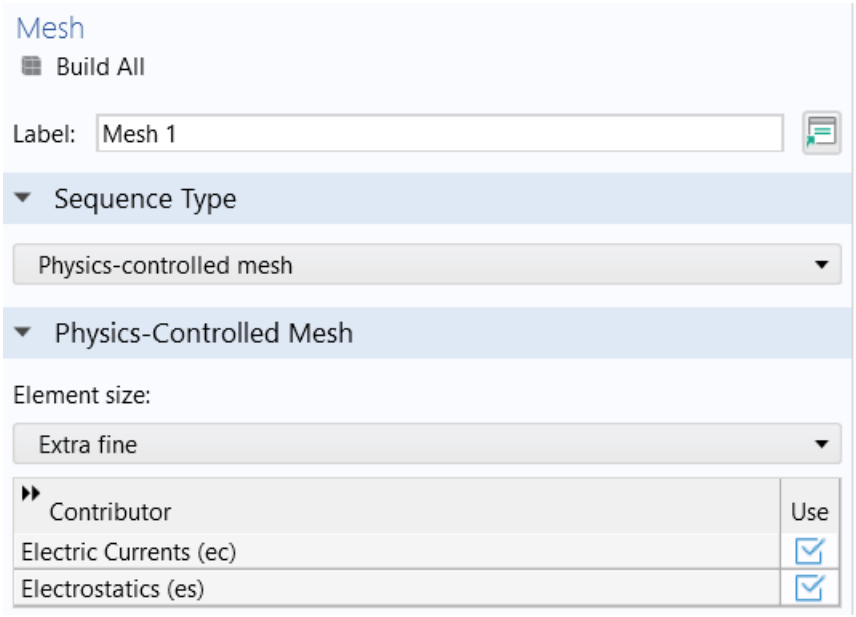

Figure 31. Finite element (FEA) mesh parameters, utilizing extra fine element size.

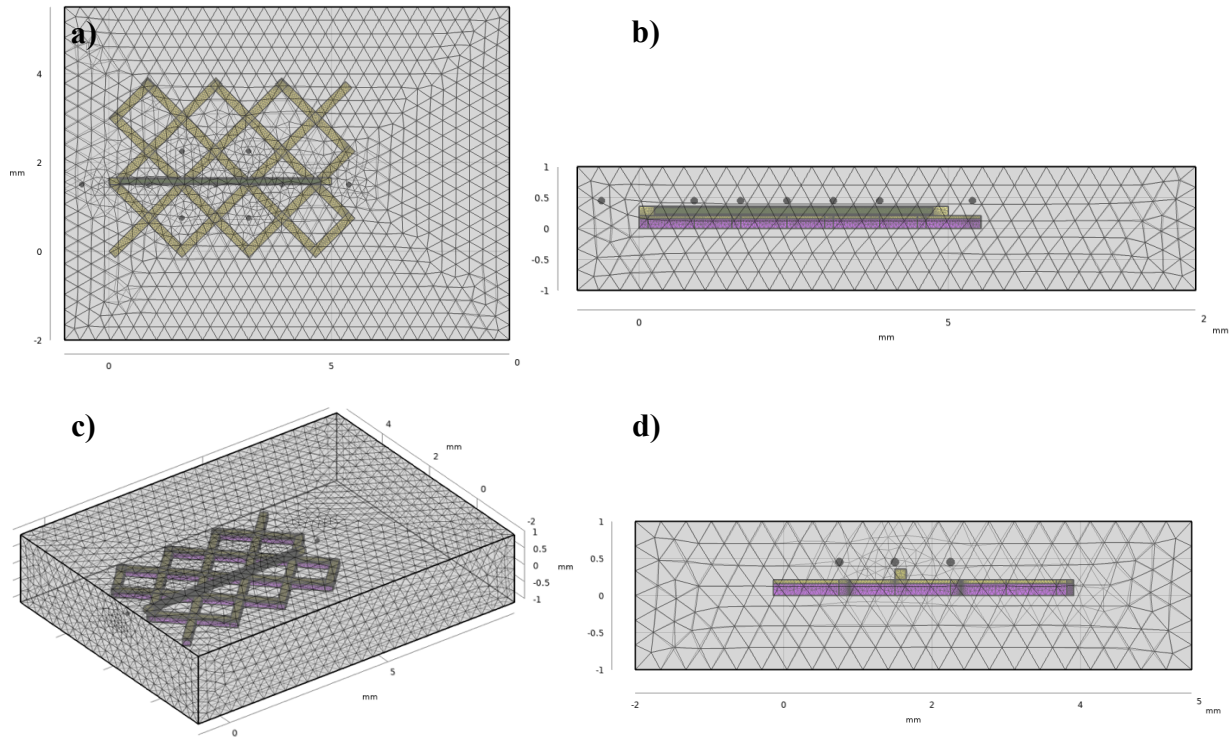

Figure 32. FEA mesh element visualization with **a)** xy-axis, **b)** xz-axis, **c)** orthogonal and **d)** yz-axis views.

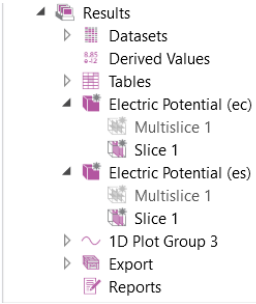

Figure 33. Workflow with 2D slices of electric potential (ec and es) results.

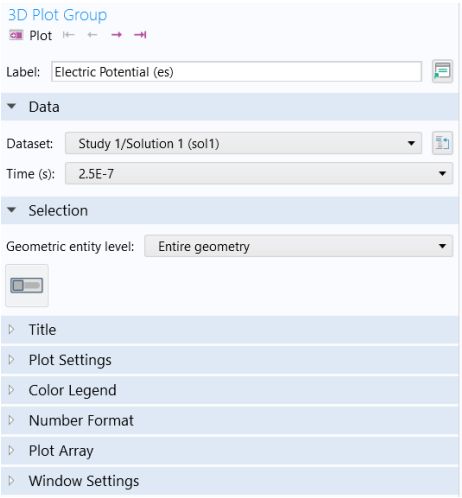

Figure 34. 3D plot settings for electric potential (es) at 2.5E-7 timepoint.

a)

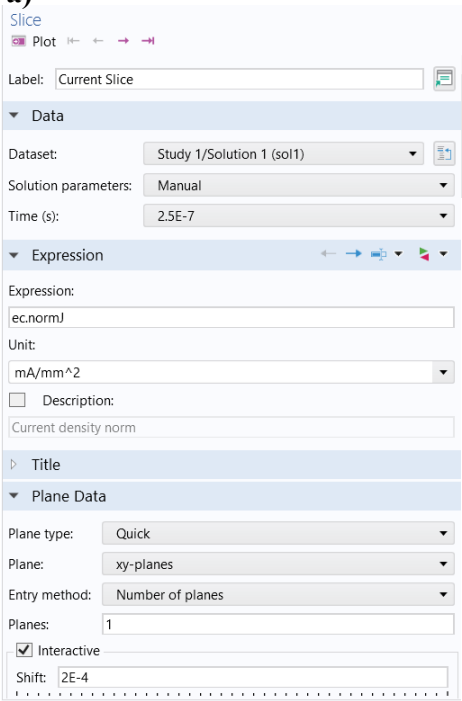

b)

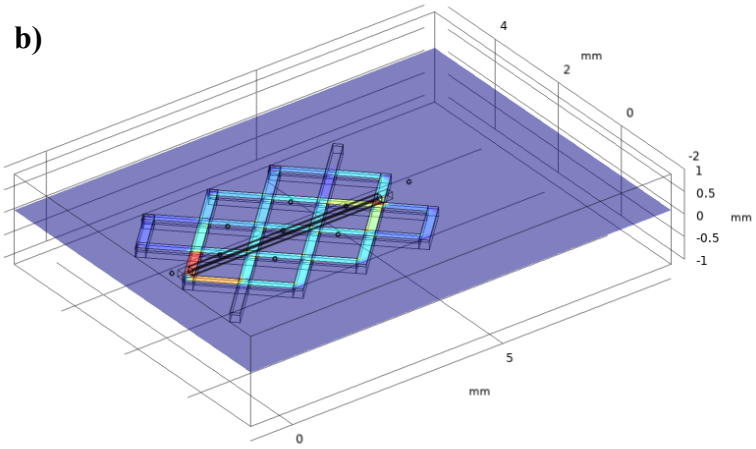

Figure 35. a) Electric current (mA/mm^2) 2D slice to show **b)** current through 3D model.

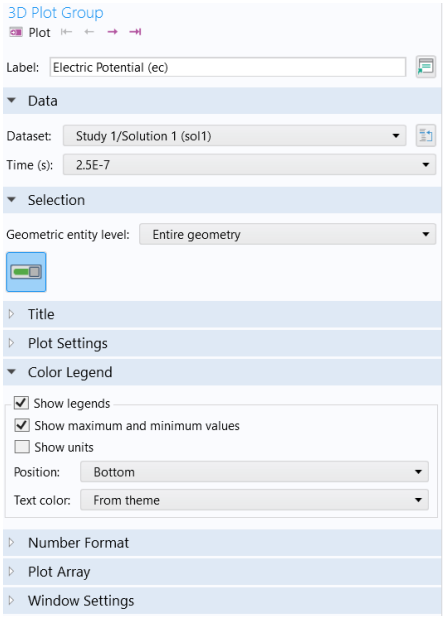

Figure 36. 3D plot settings for electric potential (ec) at 2.5E-7 timepoint.

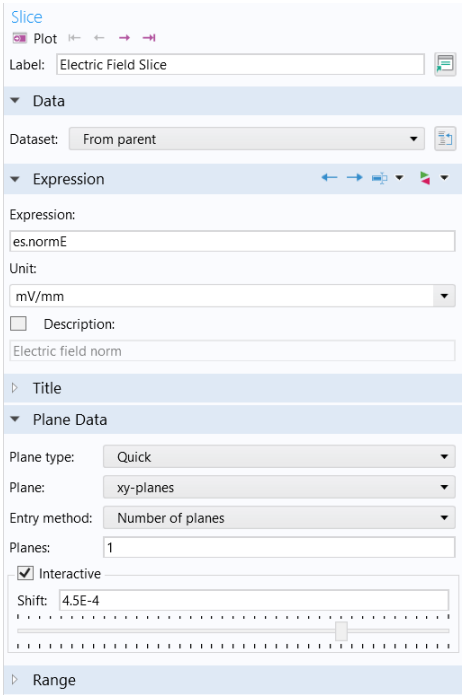

Figure 37. a) Electric current (mV/mm) 2D slice to show **b)** electric field through 3D model.